Geological Magazine

www.cambridge.org/geo

Original Article

Cite this article: Chaudhuri A, Chatterjee A, Banerjee S, and Ray JS (2021) Tracing multiple sources of sediments using trace element and Nd isotope geochemistry: provenance of the Mesozoic succession in the Kutch Basin, western India. *Geological Magazine* **158**: 359–374. https://doi.org/10.1017/S0016756820000539

Received: 17 November 2019
Revised: 1 March 2020
Accepted: 11 May 2020
First published online: 10 June 2020

Keywords:
Kutch Basin; Mesozoic; Nd isotope; Sr isotope ratio; provenance; trace elements

Author for correspondence:
Santanu Banerjee, Email: santanu@iitb.ac.in

CAMBRIDGE UNIVERSITY PRESS

Tracing multiple sources of sediments using trace element and Nd isotope geochemistry: provenance of the Mesozoic succession in the Kutch Basin, western India

Angana Chaudhuri[1], Anirban Chatterjee[2], Santanu Banerjee[1] and J.S. Ray[3]

[1]Department of Earth Sciences, Indian Institute of Technology Bombay, Powai, Mumbai 400076, India; [2]Department of Geology, Presidency University, Kolkata 700073, India and [3]Geosciences Division, Physical Research Laboratory, Navrangpura, Ahmedabad 380009, India

Abstract

An integrated approach involving Sr–Nd isotope, trace and rare earth element analyses tracks multiple sources of the Mesozoic sediments of the Kutch Basin at the western continental margin of India. High $(^{87}Sr/^{86}Sr)_t$ (ratio at time of deposition), negative ε_{Nd} and high concentrations of large-ion lithophile elements (LILEs) indicate the upper continental source. Ratios of Nb/Ta and Zr/Hf suggest sedimentary and felsic igneous sources of sediments. The moderate to high concentration of La, Th and Sc, light rare earth elements (LREE-) enrichment, weak negative Eu anomalies and the relationship between $\varepsilon_{Nd}(0)$ and Th/Sc indicate the dominantly felsic composition of source rocks. However, low contents of Th, low values of $(^{87}Sr/^{86}Sr)_t$ and depleted mantle model age $T_{DM} < 1600$ Ma indicate input from a younger mafic source. Increasing concentrations of Zr, Hf and Nd isotopes and a gradual increase in mean T_{DM} from the older to the younger formations indicate erosional unroofing at the source terrain. The increasing $(^{87}Sr/^{86}Sr)_t$ through time relates to increased weathering of the source rock. The overwhelmingly southwesterly palaeocurrent direction of current-generated sedimentary structures, and the mean T_{DM} ages trace suggest source areas of the Kutch Basin to Precambrian rocks in the north and NE of this basin. The T_{DM} ages highlight the dominance of late Palaeoproterozoic source rocks. Nd isotope composition indicates that Proterozoic rocks of Marwar Supergroup and Erinpura Granite, in particular, served as main sediment contributors for the Mesozoic sediments in Kutch. We therefore conclude that the Mesozoic sediments in the Kutch Basin are predominantly of late Palaeoproterozoic age with lesser inputs from rocks of early Mesoproterozoic and early Palaeoproterozoic age.

1. Introduction

Sedimentary successions in pericratonic rift basins preserve the evolutionary history of adjacent cratons and orogenic belts (Dickinson & Suczek, 1979; Dickinson, 1988). Provenance interpretations of these sedimentary successions contribute to the understanding of tectonic setting, climate, extent of weathering and drainage patterns during the time of deposition (Nesbitt & Young, 1982; Algeo & Maynard, 2004; Tribovillard *et al.* 2006; Hofer *et al.* 2013; Verma & Armstrong-Altrin, 2016; Armstrong-Altrin *et al.* 2019). However, temporal provenance shifts often remain untraceable because of their effects being masked by simultaneous sediment supply from multiple sources. This can be resolved only when mineralogical and geochemical variations in a sedimentary formation are correlated not only to probable sources but also to time. Due to their limited mobility during weathering and transportation, many trace elements, including rare earth elements (REEs), present in the clastic sedimentary rocks are useful in tracking dispersal of sediments (McLennan *et al.* 1983; Bhatia & Crook, 1986; Armstrong-Altrin & Verma, 2005; Armstrong-Altrin *et al.* 2013, 2018; George & Ray, 2017; Ramos-Vázquez & Armstrong-Altrin, 2019). The concentrations of trace elements and Sr and Nd isotopic composition provide information about the chemical composition and age of mantle derivation (or duration of crustal residence) of the source rocks. The integrated approach of using trace-element content, Nd isotope model ages and Sr isotope ratios is therefore likely to resolve secular shifts in the sedimentary source. The result may further enlighten us about the related plate tectonic setting.

The *c.* 3000 m thick Mesozoic succession in the Kutch Basin, western India is taken as a test case here. The choice is prompted by the fact that the secular shift in sediment contributing source has already been suggested for this succession based on petrographic modal analysis and major-element composition (Chaudhuri *et al.* 2020). However, the present approach moves forwards to the compositional make-up of the source rocks of specific time ranges. The main

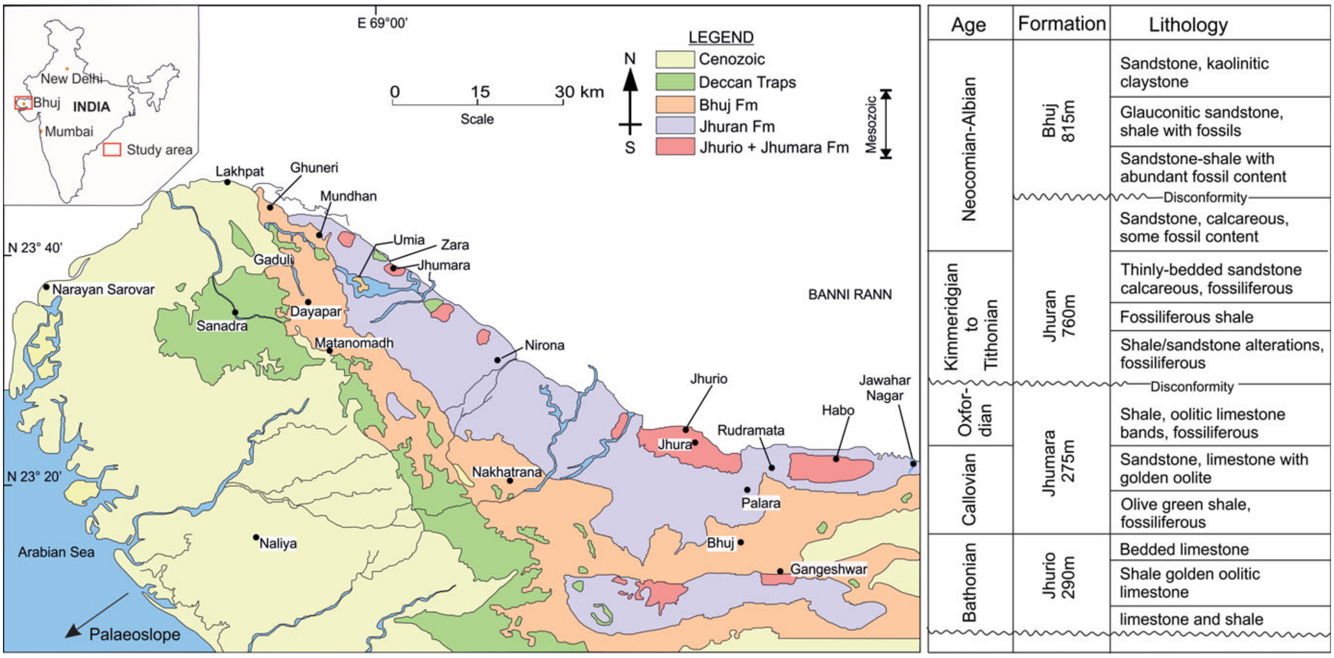

Fig. 1. (Colour online) Geological map of Kutch mainland showing extents of Cenozoic and Mesozoic outcrops (after Biswas, 1977, 1981). Mesozoic succession of the Kutch Basin, western India (after Biswas, 1977, 1981).

objective of this work is to determine the lithology and age of the source rock of Mesozoic sediments in Kutch. For this purpose, we use geochemical (trace elements) and isotopic (Sr–Nd) fingerprinting.

2. Geological setting

During the Late Jurassic Period, after the break-up of eastern Gondwana from its western counterpart, the earlier-formed Kutch Basin remained attached to the Indian subcontinent. Madagascar remained with western India until 88–90 Ma (Storey *et al.* 1995; Torsvik *et al.* 1998) while Seychelles split at *c.* 63 Ma (Collier *et al.* 2008). The Kutch Basin is a proven petroliferous basin at the western continental margin of India formed by the reactivation of primordial faults along the Aravalli–Delhi fold belt during the Gondwanaland break-up (Biswas, 1982, 1987, 2005). During the syn-rift to early post-rift stage, the Kutch Basin accumulated Upper Triassic – Lower Cretaceous mixed siliciclastic and carbonate sediments of thickness *c.* 3000 m (Biswas, 1982, 1987). The post-rift Cenozoic succession consists of mixed carbonate siliciclastic intervals (Biswas, 1981; Banerjee *et al.* 2012*a*, *b*; Saraswati *et al.* 2018). The Kutch Basin remained surrounded by Nagar Parkar Igneous Suite to the north, Bhilwara, Aravalli and Delhi Supergroups to the NE, Dharwar Supergroup to the south and Central Indian Tectonic Zone (CITZ) to the east. The Aravalli highlands to the east and the Nagar Parkar Ridge to the north are traditionally considered as source areas of the Mesozoic sediments in the Kutch Basin (Ahmad & Bhat, 2006; Ramakrishnan & Vaidyanadhan, 2008; Ahmad *et al.* 2014; Valdiya, 2015). The E–W-trending faults result in a series of uplifts exposing the Mesozoic sections in Island Belt Uplift (comprising Patcham, Khadir, Bela and Chorad islands), Wagad Uplift and Kutch Mainland Uplift (Biswas, 1980, 2005) (Fig. 1).

The Mesozoic stratigraphy of the Kutch Mainland Uplift comprises Jhurio, Jhumara, Jhuran and Bhuj formations in ascending order of succession overlying the basement rocks, separated by a basal granite–cobble conglomerate (Biswas & Deshpande, 1968; Biswas, 1987) (Fig. 1). The marine Jhurio Formation (Bathonian–Callovian) rests unconformably on the Precambrian basement and mainly comprises limestone and minor shale. The overlying Jhumara Formation (Oxfordian) consists of argillaceous sediments at the base, and limestone and minor sandstone beds at the top (Biswas, 2005). The shallow-marine Jhuran Formation (Kimmeridgian–Tithonian), unconformably overlying the Jhumara Formation, consists primarily of sandstone–shale alternations and it is divided into three constituent members based on three coarsening-upwards cycles of depositions (Arora *et al.* 2015, 2017). The youngest Bhuj Formation (Valanginian–Albian), consisting exclusively of sandstone and shale, was deposited in fluvio-deltaic conditions (Biswas, 1991). Several workers reported a predominantly south-westerly palaeocurrent pattern for the entire Mesozoic sequence (Biswas, 1991, 1993, 2005; Mandal *et al.* 2016; Arora *et al.* 2017; Desai & Biswas, 2018).

3. Methods

Samples for the present study were collected from different locations in the Kutch Mainland Uplift, namely Zara, Nirona, Palara, Bhuj, Yaksh, Rukmavati, Gangeshwar and Tapkeshwar. The majority of the collected samples from the oldest Jhurio Formation contain a significantly high amount of calcareous fragments and were therefore not included in the current study. Besides, pore-filling and replacive carbonate cements are abundant within sandstones in Jhumara, Jhuran and Bhuj formations, whereas they are absent from the associated shales in these formations (Chaudhuri *et al.* 2018). We have therefore mainly selected shale samples from Jhumara, Jhuran and Bhuj formations along

https://doi.org/10.1017/S0016756820000539 Published online by Cambridge University Press

with two sandstone samples from the Bhuj Formation because of the negligible amounts of carbonate cementation in them. In total, 15 samples from Jhumara Formation, 53 samples from Jhuran Formation and 17 samples from Bhuj Formation were analysed for the present investigation. The Jhuran Formation is considerably thick and is mapped by previous workers up to the Member level in the Kutch Mainland. A large number of studied samples therefore belong to the Jhuran Formation. For trace-element and REE concentrations, *c.* 50 mg of each sample powder was used to prepare sample solutions with 5 mL of 1 ng mL^{-1} ^{103}Rh solution added as an internal standard. From this stock solution, 5 mL was diluted to 50 mL using deionized water and analysed at CSIR-NGRI, Hyderabad, using a high-resolution inductively coupled plasma mass spectrometer (HR-ICP-MS) (Nu Instruments Attom, UK). Chinese standard reference material GSR-5 was used to check the accuracy and precision of measurements. Some of the trace-element data (sample series JP, NP and BP) were generated at the Physical Research Laboratory, Ahmedabad, India using a Thermo X-Series Q-ICP-MS. For this, carbonate and organic matter were removed from powdered samples before being dissolved in HF-HNO_3. Analyses were carried out in 2% HNO_3 sample solutions and BHVO-2 standard (from USGS) was used for calibration as well as for checking the accuracy and precision of measurements. Reproducibility at 2σ level was ≤3% for REEs and ≤6% for all other trace elements (Chatterjee & Ray, 2017, 2018).

For Sr–Nd isotopic ratio analyses at the Physical Research Laboratory, Ahmedabad, India, the samples were dissolved following the standard HF-HNO_3-HCl dissolution protocol for silicate rocks (e.g. Awasthi *et al.* 2010). Sr was separated from other REEs by cation exchange column chromatography while Nd was separated from other REEs using Ln-specific resin from Eichrom with dilute HCl (0.18 N) as elutant (Dickin, 2000; Awasthi *et al.* 2010). ^{87}Sr/^{86}Sr and ^{143}Nd/^{144}Nd were measured using a Thermo Neptune multi-collector (MC) ICP-MS (Awasthi *et al.* 2014). The measured ^{87}Sr/^{86}Sr and ^{143}Nd/^{144}Nd ratios were corrected for mass fractionation using ^{86}Sr/^{88}Sr of 0.1194 and ^{146}Nd/^{144}Nd of 0.7219. Average measured ^{143}Nd/^{144}Nd for an internal laboratory standard (Merck Nd) was 0.511705 ± 27 (2σ, $n = 56$). The average ^{143}Nd/^{144}Nd for BHVO-2, measured regularly during our analyses, is 0.512967 ± 0.000008 ($n = 10$; ±0.2 in ε_{Nd} units at 2σ). Further details of analytical protocols and data presentation for comparison are provided in Chatterjee & Ray (2017, 2018).

4. Results

4.a. Trace-element composition

Trace-element concentrations of samples from Jhumara, Jhuran and Bhuj formations are presented in Tables 1–5. Concentrations of most trace elements, especially that of large-ion lithophile elements (LILEs), are higher in these samples compared with the average shale composition (Wedepohl, 1971), except for Ni and Sc. The Lower Member of the Jhuran Formation possesses the highest average ΣREE of *c.* 317 ppm. The Upper Continental Crust (UCC) normalized trace-element concentrations in these samples are either enriched, depleted or UCC-equivalent (Fig. 2). Ba, U, Pb and Sr exhibit prominent depletion with increasing Sr depletion in younger formations. Th shows enrichment for the entire Mesozoic record. However, Nb and Ta show enrichment. The Lower Jhuran sediments show an increase in Zr and Hf, whose magnitude diminishes towards the top of the

Table 1. Trace-element concentrations of samples from Jhumara Formation. CN – chondrite-normalized

Elements	JM1	JM2	JM3	JM4	JM5	JM6	JM8	JM9	JM11	JM12	JM13	JM14	JM15	JM16	JM17	Ave
Sc	14.5	15.9	13.4	13.9	11.9	11.1	18.1	7.9	19.5	21.9	24.0	19.6	20.6	21.2	15.1	16.6
V	169.9	139.9	116.0	111.7	152.2	109.1	164.7	87.2	170.6	196.9	209.3	189.8	177.5	198.8	134.5	155.2
Cr	138.9	132.5	108.9	97.3	107.3	130.0	121.3	93.8	127.3	131.2	140.9	130.7	133.1	139.4	108.6	122.8
Co	20.3	21.3	19.5	18.8	6.4	15.9	22.3	11.9	19.0	20.7	20.7	20.0	7.4	23.2	6.8	17.0
Ni	48.1	44.2	35.1	33.4	38.2	45.2	36.4	28.0	39.3	44.7	46.3	43.4	35.3	47.6	29.3	39.6
Cu	45.4	42.4	36.6	27.8	28.8	41.9	31.1	20.9	62.2	40.1	41.2	39.5	23.8	40.1	18.8	36.0
Zn	89.2	84.3	48.2	26.8	117.9	73.3	36.3	36.5	56.6	44.2	38.4	49.3	24.9	54.1	25.8	53.7
Ga	37.4	31.2	26.1	25.5	27.4	15.8	24.8	11.6	22.2	27.2	29.8	24.1	27.2	25.7	17.8	24.9
Rb	106.2	108.0	97.0	90.7	91.4	81.6	78.7	62.9	110.2	122.7	133.4	112.1	131.1	130.5	96.7	103.5
Sr	164.9	321.9	210.7	315.9	181.4	200.7	125.8	129.2	107.3	119.6	108.9	100.4	145.9	105.0	206.9	169.6
Y	22.4	27.6	21.2	27.2	8.6	19.5	25.9	13.5	22.6	20.1	24.6	20.9	18.1	19.6	13.9	20.4
Zr	255.4	312.4	272.7	233.4	188.0	384.5	272.2	246.2	267.4	229.1	249.2	229.7	210.2	206.2	172.4	248.6
Nb	29.3	27.8	24.5	23.2	24.2	18.6	26.5	15.7	22.6	23.7	26.8	23.1	24.2	22.9	16.9	23.3
Cs	8.7	6.4	5.0	5.0	7.3	3.8	7.4	2.9	7.1	8.8	9.4	7.7	9.7	8.8	6.4	7.0

(Continued)

https://doi.org/10.1017/S0016756820000539 Published online by Cambridge University Press

Table 1. (*Continued*)

Elements	JM1	JM2	JM3	JM4	JM5	JM6	JM8	JM9	JM11	JM12	JM13	JM14	JM15	JM16	JM17	Ave
Ba	303.4	466.9	480.8	445.3	142.6	458.7	257.4	351.1	307.2	276.7	286.2	264.3	264.5	264.4	215.0	319.0
La	51.3	64.0	46.1	55.9	28.2	41.2	40.9	28.6	35.7	38.2	42.4	34.8	38.1	33.9	24.7	40.3
Ce	153.0	152.1	99.4	133.0	87.0	96.8	105.9	72.1	69.5	84.0	84.9	74.0	70.8	66.6	47.0	93.1
Pr	11.6	14.5	9.3	13.0	6.0	9.3	9.5	6.7	7.3	8.4	8.8	7.3	7.1	6.9	4.9	8.7
Nd	40.6	51.5	31.3	46.9	20.2	31.9	32.9	23.3	24.5	28.9	29.9	25.0	22.6	23.3	16.2	29.9
Sm	7.7	9.6	5.5	9.1	3.4	5.9	6.3	4.3	4.5	5.2	5.6	4.5	3.8	4.2	2.9	5.5
Eu	1.4	1.9	1.1	1.9	0.6	1.0	1.3	0.8	0.8	1.0	1.1	0.9	0.7	0.8	0.6	1.1
Gd	6.0	7.5	4.7	7.4	2.3	4.7	5.3	3.4	3.8	4.1	4.7	3.7	3.1	3.6	2.4	4.5
Tb	1.0	1.2	0.8	1.1	0.4	0.8	0.9	0.5	0.7	0.7	0.8	0.7	0.6	0.7	0.4	0.8
Dy	4.9	6.1	4.4	5.8	1.9	3.9	5.2	2.8	4.1	4.1	4.7	3.9	3.2	3.7	2.5	4.1
Ho	1.0	1.2	0.9	1.1	0.4	0.8	1.1	0.5	0.9	0.9	1.1	0.9	0.8	0.8	0.6	0.9
Er	2.7	3.4	2.6	3.0	1.2	2.3	3.2	1.6	2.8	2.7	3.2	2.7	2.3	2.5	1.8	2.5
Tm	0.4	0.5	0.4	0.4	0.2	0.3	0.5	0.2	0.4	0.4	0.5	0.4	0.3	0.4	0.3	0.4
Yb	2.8	3.5	2.8	3.0	1.5	2.5	3.6	1.7	3.1	2.9	3.4	2.9	2.6	2.7	2.0	2.7
Lu	0.5	0.6	0.5	0.5	0.3	0.4	0.6	0.3	0.5	0.5	0.6	0.5	0.4	0.4	0.3	0.4
Hf	6.0	7.2	6.2	5.5	4.4	8.8	6.4	5.8	7.9	6.8	7.4	6.9	6.4	6.1	5.1	6.5
Ta	2.3	2.2	1.9	2.0	1.8	1.6	2.1	1.2	1.8	2.0	2.1	1.8	1.7	1.8	1.4	1.8
Pb	21.4	19.1	16.2	15.1	10.6	15.9	16.7	10.8	26.1	34.6	23.4	23.3	19.1	22.1	13.2	19.2
Th	25.5	23.6	19.6	18.9	12.9	17.8	17.6	12.3	17.8	17.9	19.9	18.4	16.0	18.1	12.3	17.9
U	5.4	4.1	3.5	3.5	1.9	2.8	2.4	2.0	2.3	2.2	2.5	2.3	2.3	2.2	1.6	2.7
La/Th	2.0	2.7	2.4	3.0	2.2	2.3	2.3	2.3	2.0	2.1	2.1	1.9	2.4	1.9	2.0	2.2
Sc/Cr	0.1	0.1	0.1	0.1	0.1	0.1	0.1	0.1	0.2	0.2	0.2	0.2	0.2	0.2	0.1	0.1
∑REE	284.9	317.4	209.7	282.2	153.7	201.9	217.1	146.9	158.6	182.1	191.5	162.2	156.6	150.7	106.7	194.8
$(Gd/Yb)_{CN}$	1.7	1.7	1.3	2.0	1.2	1.5	1.2	1.6	1.0	1.2	1.1	1.0	1.0	1.1	1.0	1.3
Eu/Eu*	0.6	0.7	0.7	0.7	0.7	0.6	0.7	0.6	0.6	0.7	0.7	0.6	0.6	0.7	0.7	0.7

Table 2. Trace-element concentrations of samples from Lower Member, Jhuran Formation. CN – chondrite-normalized

Elements	L1	L2	L3	L4	L5	L6	L7	L8	L9	L10	L11	L12	L15	L16	L17	L18	Ave
Sc	15.0	16.1	10.4	17.3	16.2	16.3	18.9	18.6	10.3	19.7	15.4	12.3	15.6	15.1	16.6	17.9	15.7
V	132.8	109.9	90.1	87.2	139.9	129.4	123.5	158.9	95.4	148.3	134.9	76.4	145.2	106.4	116.3	118.9	119.6
Cr	125.8	105.0	77.9	91.9	141.3	130.9	117.8	136.0	91.9	109.5	126.3	73.2	124.2	107.4	104.7	111.7	111.0
Co	20.7	23.5	17.4	27.8	20.4	21.2	23.0	24.6	11.1	15.0	19.9	15.1	17.3	24.1	24.5	20.3	20.4
Ni	47.3	47.3	38.5	57.1	65.8	63.5	51.8	49.1	35.5	50.7	43.0	34.6	48.0	60.1	52.4	46.1	49.4
Cu	60.5	48.7	47.0	60.0	131.9	124.7	54.1	63.5	43.1	90.7	56.0	34.4	62.0	51.1	47.7	53.8	64.3
Zn	144.5	113.6	94.6	175.5	155.7	218.2	972.8	95.0	146.8	170.0	128.5	64.0	149.9	88.6	86.4	80.1	180.3
Ga	28.0	32.9	23.8	36.2	26.6	23.9	33.9	28.6	25.1	24.3	23.6	32.2	28.2	28.1	33.4	30.4	28.7
Rb	113.6	113.8	98.6	105.2	106.0	102.3	110.5	103.1	103.0	94.0	107.0	117.7	113.8	108.1	107.5	107.5	107.0
Sr	237.3	212.4	149.1	307.7	265.3	260.3	336.6	125.9	189.8	242.8	187.5	167.4	209.5	138.3	161.1	277.3	216.8
Y	28.8	32.4	27.7	47.3	29.2	32.8	38.3	31.6	30.6	45.6	26.3	40.2	27.8	38.1	45.1	40.7	35.2
Zr	191.6	258.9	269.3	308.4	227.9	309.8	233.9	189.8	204.2	171.3	205.7	287.8	156.3	234.3	223.5	244.5	232.3
Nb	21.2	23.7	21.6	28.6	20.7	20.4	23.0	21.2	20.5	18.7	20.3	24.1	19.8	21.9	23.3	21.5	21.9
Cs	6.7	6.0	5.0	5.4	8.0	6.2	6.5	6.1	6.1	6.5	5.5	6.5	8.4	5.7	6.3	5.6	6.3
Ba	572.3	617.6	586.7	398.2	776.1	768.3	597.0	461.1	503.0	534.6	544.0	590.7	397.1	550.5	515.2	620.6	564.6
La	72.1	64.2	72.0	61.2	99.7	88.8	71.5	53.3	58.4	61.1	56.8	60.3	61.2	56.4	61.9	65.3	66.5
Ce	138.2	116.5	133.5	113.5	195.6	165.8	137.3	98.8	108.3	116.9	106.5	106.6	112.2	108.0	116.8	126.0	125.0
Pr	19.4	16.6	17.4	15.6	27.5	22.7	19.5	13.5	14.3	17.2	14.7	15.4	15.9	16.1	17.0	18.0	17.6
Nd	69.9	59.8	60.8	67.2	97.8	82.2	72.6	47.6	51.1	64.8	52.1	56.8	54.4	61.5	63.8	68.7	64.4
Sm	11.4	9.4	10.1	11.8	15.5	14.6	12.0	8.3	8.8	12.5	8.5	10.1	8.0	11.4	11.7	12.6	11.0
Eu	2.0	1.8	1.5	2.5	3.0	2.6	2.4	1.7	1.7	2.7	1.6	2.1	1.6	2.3	2.4	2.5	2.2
Gd	10.8	8.0	8.9	12.2	14.4	13.0	10.4	7.7	8.3	11.5	7.9	8.8	8.4	10.0	9.7	11.6	10.1
Tb	1.4	1.2	1.2	1.7	1.9	1.8	1.6	1.2	1.2	2.0	1.1	1.5	1.1	1.6	1.7	1.8	1.5
Dy	7.3	6.9	6.5	7.8	10.4	9.8	8.4	7.0	6.6	11.6	6.1	8.4	6.5	8.6	9.4	9.1	8.2
Ho	1.3	1.2	1.2	1.3	1.8	1.8	1.5	1.3	1.3	2.3	1.1	1.5	1.2	1.5	1.6	1.6	1.5
Er	3.5	3.3	3.4	3.6	5.0	5.0	4.2	3.7	3.6	6.2	3.2	3.9	3.3	4.1	4.3	4.4	4.0
Tm	0.6	0.6	0.6	0.6	0.8	0.8	0.7	0.6	0.6	1.0	0.5	0.6	0.5	0.7	0.7	0.7	0.7
Yb	3.4	3.5	3.5	4.0	4.9	4.9	4.4	3.7	3.6	6.3	3.3	4.1	3.3	4.1	4.3	4.2	4.1
Lu	0.5	0.6	0.6	0.8	0.8	0.8	0.7	0.6	0.6	1.0	0.5	0.7	0.5	0.7	0.7	0.7	0.7
Hf	5.9	8.3	7.9	7.2	10.2	13.0	7.7	5.8	6.2	6.1	5.9	9.4	4.8	7.4	7.3	8.1	7.6
Ta	1.4	1.7	1.3	1.2	1.9	1.8	1.3	1.3	1.4	1.4	1.3	1.6	1.3	1.4	1.6	1.4	1.5
Pb	23.6	28.8	18.1	21.1	34.9	27.6	28.0	21.4	23.2	23.9	23.7	23.2	26.6	26.7	25.5	23.6	25.0
Th	25.4	24.2	34.0	22.6	33.1	39.9	23.8	22.8	23.4	25.0	22.4	26.4	22.2	23.8	26.5	27.4	26.4
U	3.5	3.5	4.3	2.6	4.7	5.6	3.9	3.4	3.5	3.6	3.1	3.6	3.1	3.3	3.4	3.7	3.7
La/Th	2.8	2.7	2.1	2.7	3.0	2.2	3.0	2.3	2.5	2.4	2.5	2.3	2.8	2.4	2.3	2.4	2.5
Sc/Cr	0.1	0.2	0.1	0.2	0.1	0.1	0.2	0.1	0.1	0.2	0.1	0.2	0.1	0.1	0.2	0.2	0.1
∑REE	341.8	293.6	321.2	303.8	479.1	414.6	347.2	249.0	268.4	317.1	263.9	280.8	278.1	287.0	306.0	327.2	317.4
$(Gd/Yb)_{CN}$	2.6	1.8	2.1	2.5	2.4	2.1	1.9	1.7	1.9	1.5	1.9	1.7	2.1	2.0	1.8	2.2	2.0
Eu/Eu*	0.6	0.6	0.5	0.6	0.6	0.6	0.7	0.7	0.6	0.7	0.6	0.7	0.6	0.7	0.7	0.6	0.6

https://doi.org/10.1017/S0016756820000539 Published online by Cambridge University Press

Table 3. Trace-element concentrations of samples from Middle Member, Jhuran Formation. CN – chondrite-normalized

Elements	M1	M2	M3	M4	M5	M6	M8	M9	M10	M11	M12	M13	M14	M15	M16	M17	M18	M19	M20	M21	M22	Ave
Sc	15.2	15.9	10.9	11.6	10.2	11.7	15.9	16.5	15.7	14.5	16.0	16.1	13.9	17.6	4.4	15.6	15.9	15.9	15.4	20.6	12.8	14.4
V	121.7	120.9	112.0	105.9	115.7	99.2	121.9	128.2	136.2	146.6	137.6	141.5	116.2	146.6	164.1	155.1	117.7	116.2	123.4	171.4	115.9	129.2
Cr	139.9	112.7	106.4	100.2	108.1	101.7	118.2	105.8	114.5	129.2	117.0	124.9	109.1	100.1	131.1	127.0	105.5	100.8	109.6	129.4	91.0	113.4
Co	26.0	23.5	17.4	23.2	20.0	18.4	22.5	16.5	26.9	18.9	21.3	11.4	19.2	9.2	14.9	14.1	23.6	15.5	20.3	37.9	11.7	19.6
Ni	40.8	45.9	34.7	63.4	37.0	33.4	46.7	45.7	57.1	47.2	48.6	39.0	43.6	30.9	54.0	43.3	49.0	39.6	42.5	75.3	38.7	45.5
Cu	162.2	42.3	31.7	52.3	32.0	24.5	38.3	62.2	59.7	62.8	47.7	47.3	58.6	149.6	81.7	68.4	46.1	56.5	45.5	67.7	51.8	61.4
Zn	64.2	71.2	52.3	54.7	41.8	42.0	59.9	165.0	128.9	97.9	63.4	77.2	113.9	71.7	352.1	116.3	81.9	120.7	63.2	138.8	104.3	99.1
Ga	25.8	25.6	23.6	22.6	24.8	21.2	25.1	36.7	36.7	30.8	37.8	31.4	26.9	27.4	3.5	36.6	34.7	35.8	36.1	28.5	29.5	28.6
Rb	120.8	108.0	84.9	82.7	81.1	82.5	103.7	102.5	97.3	87.0	91.2	93.2	91.5	78.8	90.2	92.8	95.2	97.1	89.0	87.0	88.0	92.6
Sr	145.0	212.0	174.6	223.2	183.1	181.9	260.4	115.8	110.3	91.3	126.2	109.9	97.4	107.0	86.8	110.2	133.3	111.9	135.8	125.4	105.0	140.3
Y	28.9	30.8	17.2	20.1	17.3	21.6	33.3	28.3	26.7	22.6	26.9	26.4	21.1	32.3	23.4	25.5	23.3	29.3	29.8	47.6	28.9	26.7
Zr	312.8	285.6	207.6	224.9	217.9	392.0	333.3	220.1	220.6	211.0	216.9	237.1	238.0	231.8	176.6	193.4	236.6	279.7	239.5	237.9	223.3	244.6
Nb	22.5	22.2	20.7	19.7	20.8	23.3	26.4	25.5	25.7	26.4	28.1	25.9	23.0	22.6	21.9	24.7	25.9	27.4	27.1	23.1	23.7	24.1
Cs	5.6	4.6	4.5	2.9	4.9	2.9	4.5	6.5	6.4	5.6	6.0	5.8	4.9	5.0	5.5	6.2	6.1	6.6	5.2	5.1	5.8	5.3
Ba	687.0	637.5	340.1	452.1	314.0	505.3	694.7	361.5	367.6	335.4	382.4	395.7	420.4	450.2	304.1	339.5	399.1	396.0	398.8	388.3	427.4	428.4
La	43.8	55.1	43.7	38.8	41.4	45.2	49.2	55.2	58.9	55.0	66.3	51.9	55.8	60.1	45.4	56.2	52.2	60.6	64.0	57.8	60.8	53.2
Ce	91.8	122.1	108.1	95.1	114.6	112.0	109.6	107.6	111.0	101.8	124.5	91.3	100.6	113.1	88.8	107.2	90.2	116.1	118.5	118.3	113.7	107.4
Pr	9.7	12.6	9.7	9.9	9.3	10.8	11.1	15.0	14.8	13.7	14.8	11.7	13.1	15.6	12.5	14.4	11.2	15.5	14.1	16.7	15.4	12.9
Nd	34.1	44.3	33.2	36.6	31.9	38.4	39.8	57.4	52.5	47.2	53.2	40.7	45.6	55.6	44.9	51.8	38.9	55.4	50.6	64.4	54.5	46.2
Sm	7.0	8.6	5.9	7.2	5.6	6.9	8.0	10.0	8.9	7.6	10.0	7.1	7.6	9.6	7.9	8.8	7.1	9.1	9.6	12.6	9.3	8.3
Eu	1.6	1.8	1.1	1.5	1.1	1.4	1.9	2.1	1.8	1.5	2.0	1.4	1.4	2.0	1.7	1.9	1.4	1.8	1.9	2.8	1.9	1.7
Gd	6.5	7.3	4.7	5.9	4.5	5.4	7.4	10.3	8.7	7.3	8.9	6.7	7.1	8.8	9.5	9.5	6.8	8.0	8.6	12.8	8.6	7.8
Tb	1.1	1.2	0.7	0.9	0.7	0.9	1.2	1.3	1.2	1.0	1.3	1.0	1.0	1.4	1.2	1.2	1.0	1.2	1.3	2.0	1.3	1.2
Dy	6.0	6.5	3.9	4.9	3.8	4.8	6.6	6.7	6.2	5.6	6.3	5.7	5.0	8.3	6.4	6.2	5.0	6.6	6.2	10.3	7.3	6.1
Ho	1.2	1.3	0.8	1.0	0.7	1.0	1.3	1.2	1.1	1.0	1.1	1.1	0.9	1.6	1.1	1.1	1.0	1.1	1.2	1.9	1.3	1.1
Er	3.4	3.7	2.2	2.6	2.1	2.9	3.7	3.2	3.1	2.8	3.1	3.1	2.5	4.3	3.2	3.0	2.7	3.1	3.2	5.0	3.7	3.2
Tm	0.5	0.5	0.3	0.4	0.3	0.4	0.5	0.5	0.5	0.4	0.5	0.5	0.4	0.7	0.5	0.5	0.5	0.5	0.5	0.7	0.6	0.5
Yb	3.7	3.7	2.2	2.6	2.1	3.1	3.7	3.3	3.1	2.8	3.1	3.2	2.5	4.5	3.2	3.0	2.9	3.1	3.2	4.5	3.7	3.2
Lu	0.6	0.6	0.4	0.4	0.3	0.5	0.6	0.5	0.5	0.4	0.5	0.5	0.4	0.7	0.5	0.5	0.5	0.5	0.5	0.7	0.6	0.5
Hf	8.0	6.8	4.9	5.3	5.0	9.2	7.6	6.9	7.0	6.4	7.4	7.4	7.2	8.3	0.6	6.0	7.8	8.9	8.0	6.7	7.6	6.8
Ta	1.8	1.8	1.6	1.5	1.6	3.1	2.2	1.6	1.7	1.7	2.2	1.5	1.5	1.5	0.3	1.4	1.9	1.8	2.1	1.4	1.6	1.7
Pb	35.5	17.3	15.4	14.3	15.5	13.6	21.0	25.0	23.2	23.1	26.4	19.1	20.0	20.0	19.2	23.7	25.4	24.4	22.8	21.0	23.0	21.4
Th	18.3	18.3	16.6	14.1	16.8	15.9	18.3	23.6	24.8	23.7	27.0	22.7	25.2	21.5	21.3	23.9	23.8	27.2	24.2	20.9	22.4	21.4
U	3.5	3.4	2.8	2.8	2.9	3.4	3.4	3.3	3.8	3.5	4.2	3.5	3.8	3.6	3.5	3.7	3.8	4.0	4.2	3.8	3.6	3.5
La/Th	2.4	3.0	2.6	2.8	2.5	2.8	2.7	2.3	2.4	2.3	2.5	2.3	2.2	2.8	2.1	2.4	2.2	2.2	2.6	2.8	2.7	2.5
Sc/Cr	0.1	0.1	0.1	0.1	0.1	0.1	0.1	0.2	0.1	0.1	0.1	0.1	0.1	0.2	0.0	0.1	0.2	0.2	0.1	0.2	0.1	0.1
∑REE	211.2	269.3	216.8	207.8	218.4	233.8	244.7	274.2	272.2	248.2	295.8	226.0	243.8	286.4	226.8	265.0	221.4	282.7	283.3	310.4	282.5	253.4
$(Gd/Yb)_{CN}$	1.4	1.6	1.7	1.8	1.7	1.4	1.6	2.5	2.2	2.1	2.3	1.7	2.3	1.6	2.4	2.6	1.9	2.1	2.2	2.3	1.9	2.0
Eu/Eu*	0.7	0.7	0.7	0.7	0.7	0.7	0.7	0.6	0.6	0.6	0.7	0.6	0.6	0.7	0.6	0.6	0.6	0.6	0.6	0.7	0.7	0.7

https://doi.org/10.1017/S0016756820000539 Published online by Cambridge University Press

Table 4. Trace-element concentrations of samples from Upper Member, Jhuran Formation. CN – chondrite-normalized

Elements	U1	U2	U3	U4	U5	U6	U7	U8	U9	U10	U11	U12	U13	U14	U15	U16	Ave
Sc	7.6	7.4	11.0	12.3	8.0	6.6	10.4	8.7	13.5	10.6	9.2	8.4	7.2	15.5	10.3	13.6	10.0
V	125.5	119.5	125.4	109.7	95.2	100.9	118.3	111.3	137.6	122.5	155.0	149.0	159.2	141.0	122.2	129.7	126.4
Cr	100.7	106.4	113.6	96.9	85.8	86.4	101.3	90.2	106.0	97.2	121.7	126.2	128.5	117.6	106.6	109.7	105.9
Co	16.0	5.8	5.5	8.1	6.4	11.2	8.1	8.3	11.7	7.9	24.3	14.9	12.4	11.3	11.6	16.9	11.3
Ni	48.1	31.9	26.7	32.6	25.0	24.2	25.5	26.6	35.1	26.8	80.2	42.5	43.9	33.5	30.5	31.5	35.3
Cu	40.2	31.2	30.0	26.1	22.4	21.6	27.0	27.4	35.4	39.5	40.3	42.8	27.3	29.8	26.8	30.3	31.1
Zn	145.4	108.2	36.0	100.0	63.2	39.6	39.9	53.5	39.3	56.6	61.3	60.2	46.7	40.0	49.7	33.1	60.8
Ga	20.5	20.9	24.6	23.8	19.2	19.6	23.5	21.5	24.9	23.6	28.2	28.5	29.8	27.3	24.8	26.0	24.2
Rb	69.9	83.7	91.6	84.6	68.2	70.1	96.6	58.5	90.0	79.0	57.0	72.3	19.7	104.0	91.8	104.6	77.6
Sr	195.6	107.8	109.7	206.5	85.8	85.1	156.8	115.7	155.8	117.2	86.8	128.2	71.7	137.6	213.0	208.0	136.3
Y	12.7	11.2	13.9	21.9	9.4	9.2	15.6	9.7	21.3	14.1	8.5	14.4	10.1	25.0	16.2	22.3	14.7
Zr	218.8	221.7	226.0	199.5	226.1	174.2	199.9	188.8	204.4	187.2	207.5	257.4	226.9	230.0	262.8	234.3	216.6
Nb	20.1	22.3	25.7	22.2	21.0	20.6	23.1	22.8	22.9	23.0	23.7	24.6	25.5	22.8	21.9	22.7	22.8
Cs	2.9	3.9	4.4	5.4	2.7	2.7	7.5	3.9	6.7	4.3	6.4	6.0	5.7	5.5	4.7	5.4	4.9
Ba	220.2	181.7	233.9	289.3	177.6	165.3	185.6	159.0	228.4	201.8	120.2	253.0	75.2	514.7	346.1	470.5	238.9
La	24.5	26.4	32.5	51.0	24.3	22.1	45.2	21.3	39.8	48.8	58.5	33.2	58.7	54.7	40.0	44.0	39.1
Ce	58.5	56.8	74.4	102.6	53.5	49.9	93.5	64.8	93.1	103.2	119.1	130.0	114.3	115.1	114.9	85.2	89.3
Pr	6.2	6.6	7.7	11.8	6.2	5.6	10.7	5.0	8.9	11.1	13.4	7.5	13.1	13.0	9.5	9.9	9.1
Nd	22.1	23.2	26.7	42.2	22.0	19.8	38.3	17.3	30.7	39.4	48.8	26.5	47.3	47.6	33.7	35.1	32.5
Sm	4.4	4.5	5.0	7.6	4.1	3.7	7.0	3.2	5.9	7.0	9.2	4.9	8.6	8.9	6.4	6.3	6.0
Eu	1.0	0.9	1.0	1.6	0.8	0.7	1.4	0.6	1.2	1.5	2.1	0.9	1.9	1.9	1.3	1.4	1.3
Gd	3.6	3.5	3.9	6.9	3.2	2.9	6.3	2.6	4.9	6.3	8.8	4.1	8.1	8.3	4.9	5.8	5.3
Tb	0.6	0.6	0.6	0.9	0.5	0.5	0.8	0.4	0.8	0.8	1.2	0.6	1.0	1.1	0.8	0.7	0.7
Dy	3.0	3.0	3.4	4.7	2.7	2.5	4.3	2.3	4.5	4.2	6.6	3.2	5.8	5.7	3.9	4.2	4.0
Ho	0.6	0.6	0.7	0.9	0.5	0.5	0.8	0.5	0.9	0.8	1.3	0.6	1.1	1.1	0.8	0.8	0.8
Er	1.7	1.6	1.9	2.5	1.5	1.4	2.5	1.3	2.5	2.3	4.7	1.7	3.2	3.1	2.1	2.5	2.3
Tm	0.3	0.2	0.3	0.4	0.2	0.2	0.4	0.2	0.4	0.3	0.5	0.2	0.5	0.4	0.3	0.4	0.3
Yb	1.8	1.6	2.1	2.4	1.6	1.5	2.4	1.5	2.7	2.3	3.3	1.7	3.1	2.9	2.2	2.6	2.2
Lu	0.3	0.3	0.3	0.3	0.3	0.2	0.3	0.2	0.4	0.3	0.5	0.3	0.4	0.4	0.4	0.4	0.3
Hf	5.1	5.2	5.4	4.8	5.3	4.2	4.9	4.6	4.8	4.5	4.9	6.1	5.3	5.4	6.1	5.6	5.1
Ta	1.5	1.6	2.1	1.7	1.6	1.6	1.7	1.8	1.7	1.9	1.8	1.8	2.1	1.8	1.7	1.7	1.8
Pb	21.5	15.8	16.0	14.0	14.4	13.2	12.9	13.9	16.2	15.4	17.1	16.3	12.1	16.4	14.7	13.9	15.2
Th	13.1	14.4	16.0	17.1	14.6	12.5	15.9	13.4	17.1	16.5	7.0	16.4	12.1	21.3	17.4	19.0	15.2
U	2.6	2.5	2.5	2.4	2.4	2.1	2.4	2.2	2.4	2.3	2.8	3.2	3.0	3.2	3.2	3.1	2.6
La/Th	1.9	1.8	2.0	3.0	1.7	1.8	2.8	1.6	2.3	3.0	8.4	2.0	4.9	2.6	2.3	2.3	2.8
Sc/Cr	0.1	0.1	0.1	0.1	0.1	0.1	0.1	0.1	0.1	0.1	0.1	0.1	0.1	0.1	0.1	0.1	0.1
∑REE	128.6	129.6	160.6	235.7	121.4	111.5	213.9	121.3	196.8	228.4	277.9	215.6	267.1	264.2	221.0	199.3	193.3
$(Gd/Yb)_{CN}$	1.6	1.7	1.5	1.6	1.6	1.6	1.5	1.4	1.5	1.6	1.5	1.9	1.3	1.7	1.8	1.3	1.6
Eu/Eu*	0.7	0.7	0.7	0.7	0.7	0.7	0.7	0.7	0.7	0.7	0.6	0.6	0.6	0.7	0.7	0.7	0.7

https://doi.org/10.1017/S0016756820000539 Published online by Cambridge University Press

Table 5. Trace-element concentrations of samples from Bhuj Formation. CN – chondrite-normalized

Elements	B1	B2	B3	B4	B5	B6	B7	B8	B9	B10	B11	B12	B14	B15	B16	B17	B18	Ave
Sc	12.0	12.8	18.0	14.3	14.5	17.2	16.8	16.0	10.8	9.3	8.8	14.5	11.4	13.0	17.7	12.7	17.5	13.9
V	127.1	128.5	126.6	98.0	101.0	111.4	108.4	108.8	57.2	51.0	54.7	111.8	90.0	114.3	115.9	93.0	95.4	99.6
Cr	144.9	111.4	116.0	118.0	102.7	115.1	114.1	130.9	84.5	61.0	69.5	109.9	93.9	108.3	128.7	122.0	157.1	111.1
Co	16.1	13.7	26.6	16.4	22.9	21.3	20.5	16.5	16.1	10.6	9.1	3.4	60.3	9.6	13.8	14.6	4.1	17.4
Ni	32.2	30.6	44.6	49.6	41.1	42.2	38.3	42.9	35.9	24.6	23.9	19.2	52.6	31.8	42.1	41.5	31.5	36.7
Cu	29.5	28.7	34.8	30.4	33.9	39.0	35.1	84.9	20.4	17.0	16.7	18.2	23.1	30.7	38.5	23.4	25.2	31.1
Zn	47.1	54.1	64.1	53.1	100.0	79.0	50.7	120.8	31.6	39.8	43.1	31.9	52.1	40.3	44.5	77.2	30.8	56.5
Ga	29.5	29.3	28.1	22.6	19.0	23.6	22.5	24.2	14.0	13.6	11.3	21.3	20.8	24.5	28.3	18.0	26.7	22.2
Rb	95.3	94.2	99.0	89.6	74.4	92.5	87.4	89.3	85.8	89.3	70.8	82.5	102.3	58.0	84.1	121.7	109.1	89.7
Sr	100.2	101.8	129.3	130.4	59.1	67.9	67.3	76.2	76.4	93.9	235.4	77.9	118.1	49.6	44.3	91.7	183.2	100.2
Y	24.7	20.0	33.4	32.7	31.0	36.6	34.6	33.7	28.4	21.0	18.4	28.0	21.4	33.3	24.6	34.2	42.1	29.3
Zr	265.2	233.0	252.9	431.4	219.9	261.5	271.3	324.5	466.6	343.2	410.7	277.5	215.5	335.8	217.6	552.1	481.4	327.1
Nb	24.3	25.0	23.1	23.6	19.3	23.0	22.6	22.8	19.2	17.4	16.9	22.6	18.3	24.2	26.0	20.6	28.6	22.2
Cs	6.8	7.1	6.6	3.9	3.8	4.8	4.4	4.1	2.0	1.5	0.9	4.3	3.8	6.0	8.9	4.1	3.0	4.5
Ba	255.4	182.2	283.9	486.3	388.2	459.5	462.7	518.4	686.9	822.0	768.4	453.4	801.3	262.4	219.2	847.1	1063.3	527.1
La	57.9	47.2	63.2	69.1	45.6	60.0	55.9	63.8	44.6	41.5	59.2	52.9	40.0	62.9	61.3	52.7	83.5	56.6
Ce	143.5	137.8	146.8	154.4	84.3	109.9	102.1	112.7	78.9	74.4	107.0	99.0	91.5	107.9	114.7	96.8	148.1	112.3
Pr	12.6	10.2	13.9	15.3	10.2	13.1	12.3	13.7	9.5	9.0	12.9	11.3	9.2	12.7	11.9	11.5	17.8	12.2
Nd	44.1	35.7	49.2	53.2	36.7	47.6	44.4	49.2	33.8	32.2	45.3	40.3	33.8	44.6	41.1	41.8	62.3	43.2
Sm	8.2	6.5	9.4	9.8	7.2	9.3	8.6	9.3	6.3	5.9	7.8	7.7	6.6	7.9	7.4	7.8	11.5	8.1
Eu	1.6	1.3	1.9	1.5	1.5	1.8	1.7	1.7	1.1	1.0	0.9	1.4	1.5	1.2	1.3	1.4	2.1	1.5
Gd	6.6	5.1	8.1	7.6	6.3	7.9	7.4	7.8	5.2	4.8	5.7	6.3	5.9	6.7	5.9	7.1	9.5	6.7
Tb	1.0	0.8	1.3	1.2	1.1	1.3	1.2	1.3	0.9	0.7	0.8	1.0	0.9	1.1	1.0	1.2	1.6	1.1
Dy	5.3	4.3	7.1	6.5	5.8	6.8	6.5	6.3	4.8	3.8	3.5	5.5	4.7	5.9	5.0	6.1	7.8	5.6
Ho	1.1	0.9	1.4	1.3	1.2	1.4	1.4	1.3	1.1	0.8	0.7	1.2	0.9	1.2	1.0	1.3	1.6	1.2
Er	2.9	2.4	3.9	4.0	3.4	4.0	3.9	3.7	3.1	2.3	2.1	3.3	2.4	3.5	2.8	3.7	4.6	3.3
Tm	0.4	0.3	0.5	0.6	0.5	0.5	0.5	0.5	0.4	0.3	0.3	0.5	0.3	0.5	0.4	0.5	0.6	0.4
Yb	2.8	2.4	3.9	4.5	3.3	3.8	3.8	3.5	3.1	2.3	2.0	3.4	2.2	3.4	2.5	3.6	4.4	3.2
Lu	0.5	0.4	0.6	0.8	0.5	0.6	0.6	0.6	0.5	0.4	0.3	0.5	0.4	0.5	0.4	0.6	0.7	0.5
Hf	6.2	5.7	6.2	10.1	6.2	7.6	7.8	9.4	13.2	9.6	12.1	8.3	5.0	9.5	6.3	15.3	14.0	9.0
Ta	1.9	2.2	1.9	1.8	1.2	1.7	1.7	1.8	1.3	1.3	1.2	1.9	1.3	2.0	2.1	1.6	2.1	1.7
Pb	12.4	14.1	17.1	14.9	35.4	22.3	17.9	27.4	14.6	17.5	17.1	15.0	9.8	21.0	22.2	29.7	37.4	20.3
Th	22.4	18.9	24.3	27.0	15.5	19.9	19.9	21.6	18.8	19.2	28.0	23.2	13.7	20.4	24.2	22.2	30.2	21.7
U	4.5	4.5	5.1	5.3	3.5	4.2	4.2	4.6	3.4	2.9	3.7	4.9	4.5	4.3	4.5	5.1	6.5	4.4
La/Th	2.6	2.5	2.6	2.6	2.9	3.0	2.8	3.0	2.4	2.2	2.1	2.3	2.9	3.1	2.5	2.4	2.8	2.6
Sc/Cr	0.1	0.1	0.2	0.1	0.1	0.1	0.1	0.1	0.1	0.2	0.1	0.1	0.1	0.1	0.1	0.1	0.1	0.1
∑REE	288.5	255.3	311.3	329.8	207.6	268.0	250.3	275.3	193.4	179.3	248.6	234.3	200.4	259.9	256.6	236.0	356.3	255.9
$(Gd/Yb)_{CN}$	1.9	1.7	1.7	1.4	1.5	1.7	1.6	1.8	1.4	1.7	2.3	1.5	2.1	1.6	1.9	1.6	1.7	1.7
Eu/Eu*	0.7	0.7	0.7	0.5	0.7	0.6	0.6	0.6	0.6	0.6	0.4	0.6	0.7	0.5	0.6	0.6	0.6	0.6

https://doi.org/10.1017/S0016756820000539 Published online by Cambridge University Press

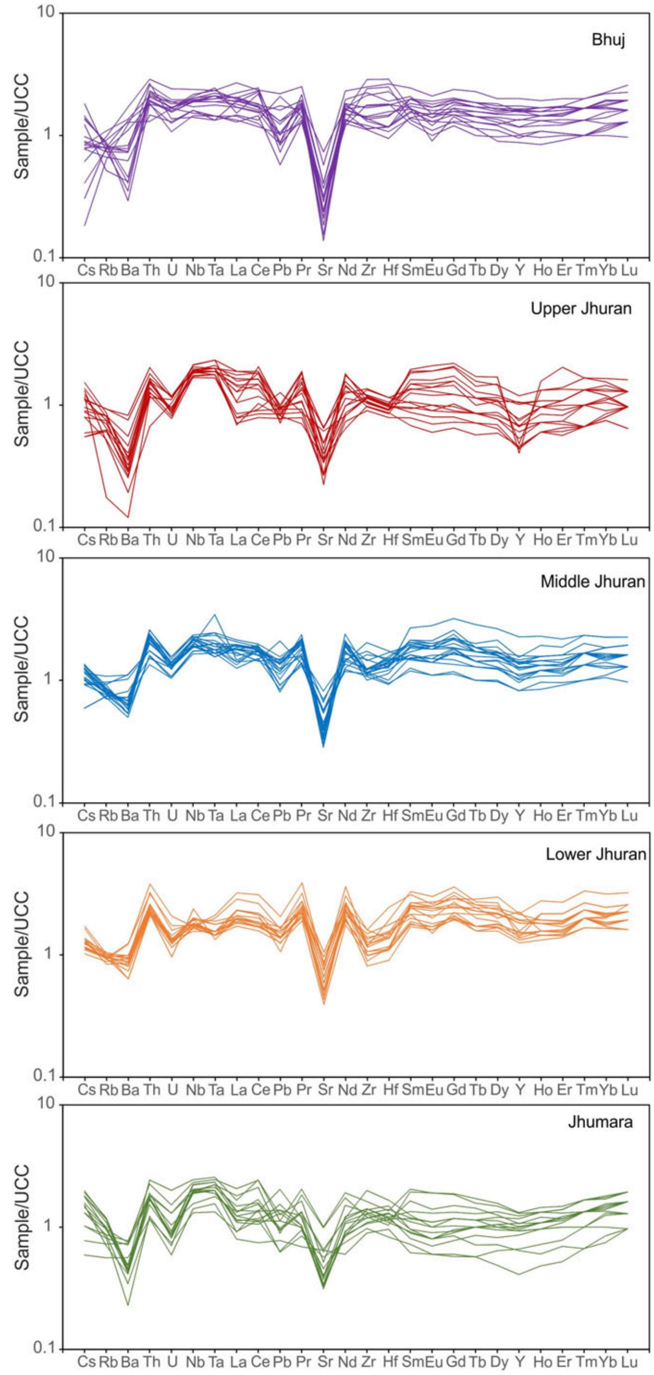

Fig. 2. (Colour online) Upper Continental Crust (UCC-) normalized trace-element patterns for samples from various formations, arranged in stratigraphic order, of the Mesozoic Kutch Basin. Normalizing values are from Rudnick & Gao (2003).

succession (Fig. 2). The Nb/Ta versus Zr/Hf of all the samples from the basin show two clusters, one group showing higher Nb/Ta and lower Zr/Hf compared with the other (Fig. 3).

Chondrite-normalized REE patterns of Jhumara, Jhuran and Bhuj samples show broadly similar characteristics, with a prominently LREE-enriched pattern, negative Eu anomaly and positive Gd anomaly (Fig. 4). These patterns broadly overlap with those of UCC and Post-Archean Australian Shale (PAAS). Weak negative

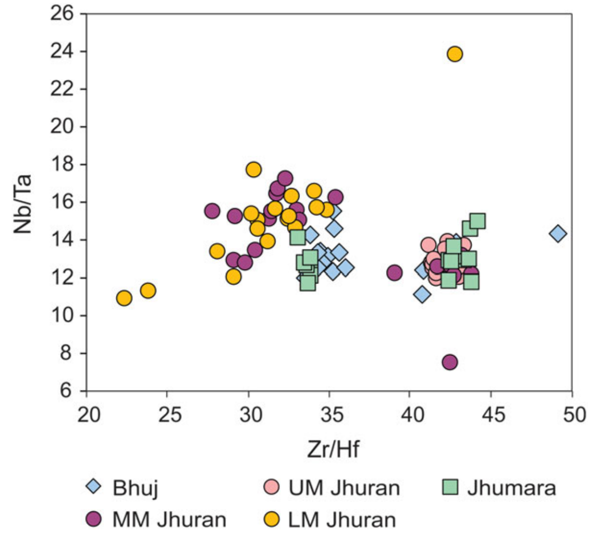

Fig. 3. (Colour online) Nb/Ta versus Zr/Hf plot for samples from the Mesozoic Kutch Basin.

Eu anomalies, $Eu/Eu^* = Eu/(Sm_{CN}{*}Nd_{CN})^{1/2}$ (where the subscript 'CN' indicates chondrite-normalized) in Jhumara, Jhuran and Bhuj samples have average values of 0.65, 0.65 and 0.61, respectively. The chondrite-normalized REE patterns for shale samples from the Jhuran Formation reveal three distinct bands for its three Lower, Middle and Upper members (Fig. 4). The samples from the Lower Member exhibit consistently high ΣREE contents, whereas those of the Upper Member show distinctly low ΣREE content. Nearly half of the samples from the Jhumara Formation exhibit REE patterns similar to those of the Upper Member of the Jhuran Formation. Samples from all three formations exhibit a low La/Th ratio (1.59–3.01 ppm); those from the Bhuj Formation exhibit the highest average (2.60). In a cross-plot of Th versus Sc, the samples from the Jhuran Formation exhibit the maximum spread of data points (Fig. 5). Most samples from Jhuran and Bhuj formations and nearly half of the samples from the Jhumara Formation bear felsic signature, while a few samples from the Jhuran (belonging to the Upper and Middle members) and Bhuj formations and most samples from the Jhumara Formation plot within the field for intermediate igneous rocks (Fig. 5) (Cullers, 2002).

Average Sc/Cr ratios for samples from Jhumara, Jhuran and Bhuj formations are 0.13, 0.12 and 0.13 respectively. In a cross-plot of La/Th versus Hf, most samples plot in the field marked for passive margin sources, but a few samples occupy the field of acidic arc sources (Fig. 6). Samples from the Lower Member of Jhuran Formation and the Bhuj Formation exhibit distinctly higher concentrations of Hf compared with samples from other formations.

4.b. Isotope composition

Samples from Jhumara, Jhuran and Bhuj formations bear continental crustal signatures. The value of $(^{87}Sr/^{86}Sr)_t$ is similar in all three formations; samples from the Bhuj Formation have the highest $(^{87}Sr/^{86}Sr)_t$ ranging over 0.73–0.76, followed by Jhuran Formation (0.72–0.75) and Jhumara Formation (0.72–0.73) (Fig. 7). All samples exhibit overlapping but negative $\varepsilon_{Nd}(0)$ and $\varepsilon_{Nd}(t)$ values, suggesting derivation from LREE-enriched mantle.

https://doi.org/10.1017/S0016756820000539 Published online by Cambridge University Press

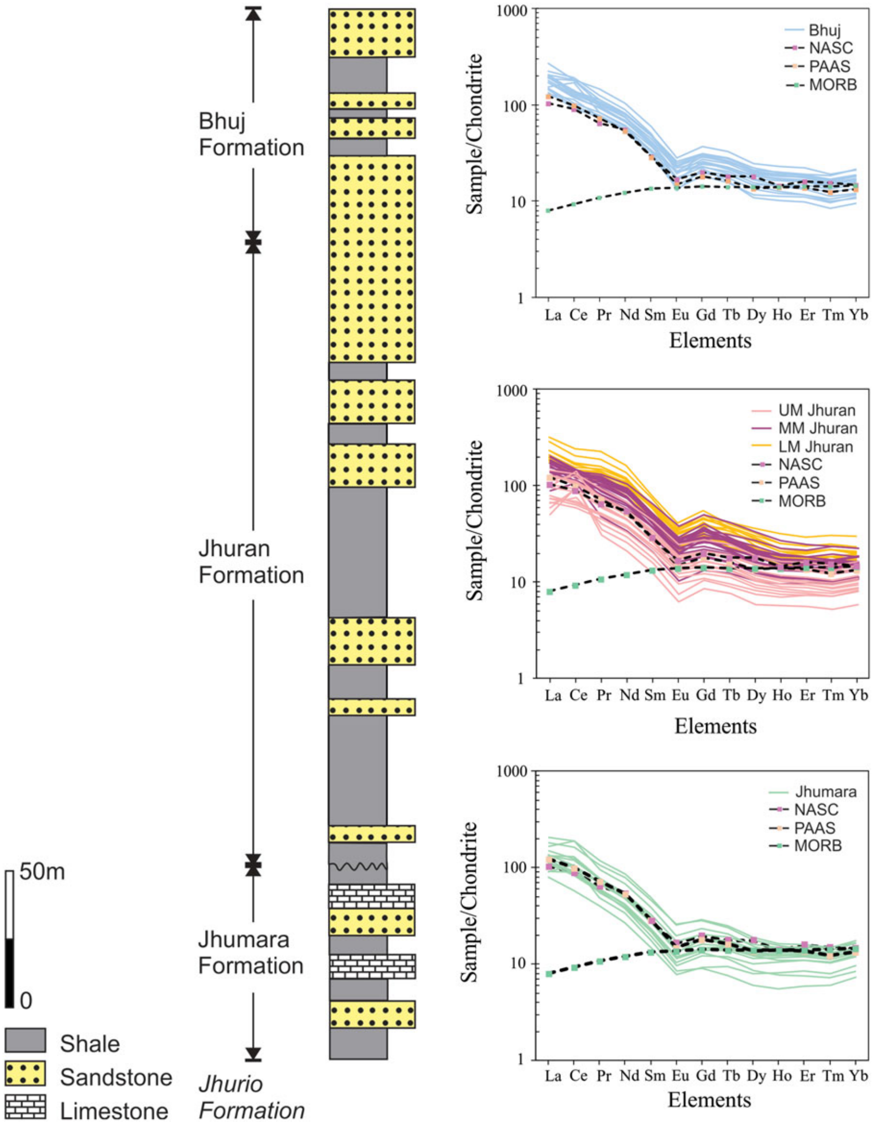

Fig. 4. (Colour online) Composite log of the Jhumara, Jhuran and Bhuj formations (adapted from Biswas, 2005; Fursich *et al.* 2005; Mandal *et al.* 2016). Chondrite-normalized REE patterns for Jhumara (lower), Jhuran (middle) and Bhuj (upper) are placed to the right of the log. Solid lines: LM – Lower Member; MM – Middle Member; UM – Upper Member. Dashed lines: MORB – mid-ocean-ridge basalt; NASC – North American Shale Composite; PAAS – Post Archean Australian Shale. Chondrite meteorite values from Boynton (1984). NASC, PAAS and MORB values from Taylor & McLennan (1985).

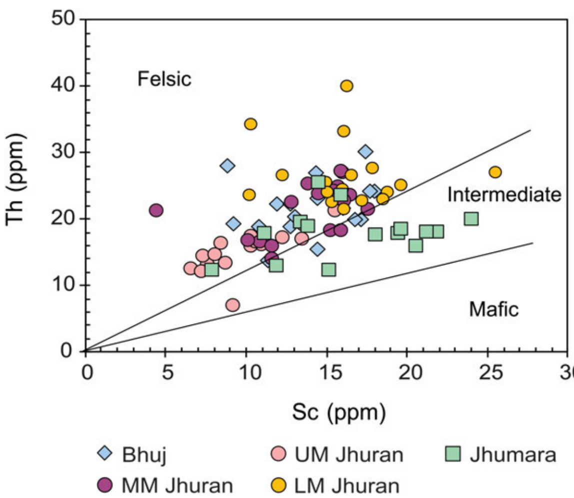

Fig. 5. (Colour online) Source-rock discrimination based on Th versus Sc plot (Cullers, 2002) for shale samples from Jhumara, Jhuran and Bhuj formations. Abbreviations as for Figure 4.

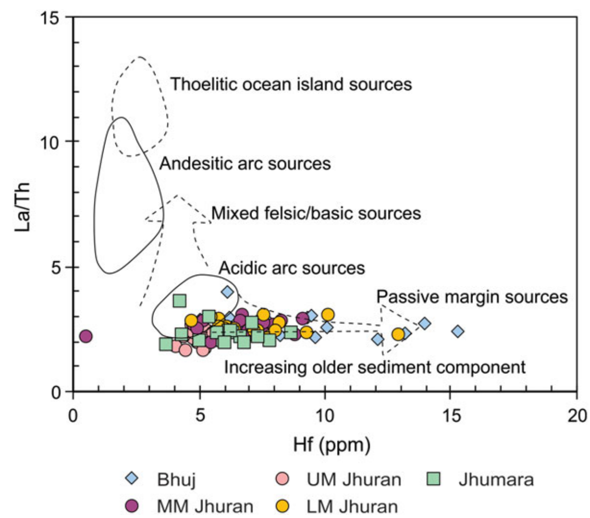

Fig. 6. (Colour online) Tectonic setting discrimination based on La/Th versus Hf (Floyd & Leveridge, 1987) for shale samples from Jhumara, Jhuran and Bhuj formations. Abbreviations as for Figure 4.

https://doi.org/10.1017/S0016756820000539 Published online by Cambridge University Press

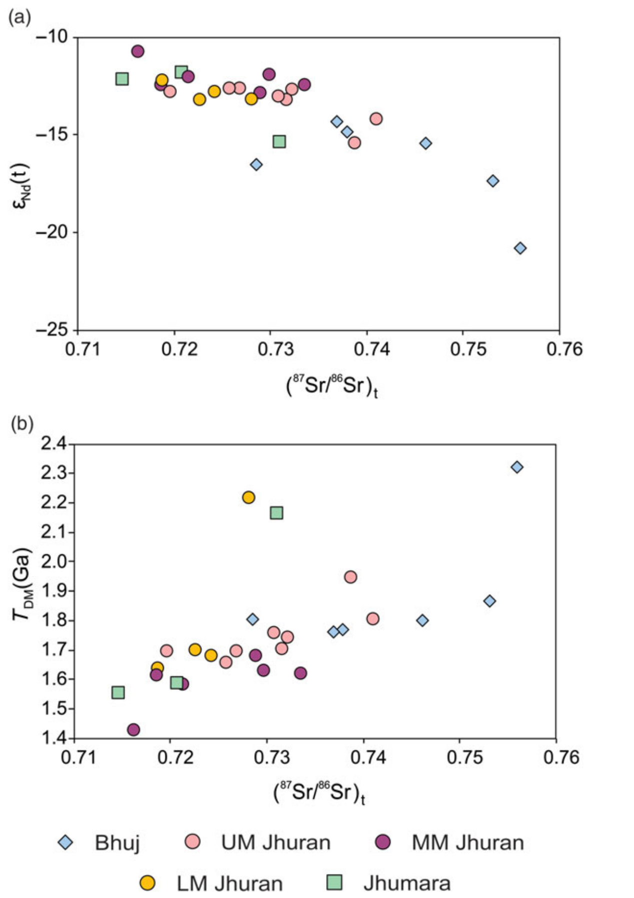

Fig. 7. (Colour online) (a) $\varepsilon_{Nd}(t)$ and (b) T_{DM} versus $(^{87}Sr/^{86}Sr)_t$ plot for shale samples from Jhumara, Jhuran and Bhuj formations. Abbreviations as for Figure 4.

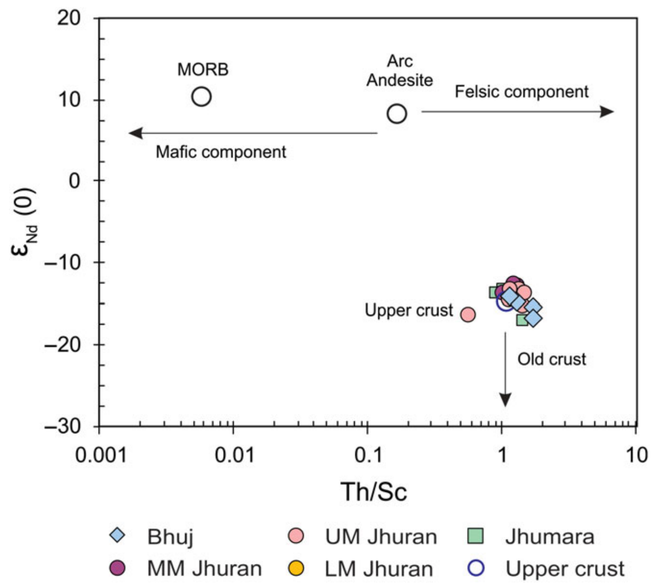

Fig. 8. (Colour online) Source-rock discrimination based on ε_{Nd} versus Th/Sc plot (McLennan *et al.* 1993) for shale samples from Jhumara, Jhuran and Bhuj Formation. Abbreviations as for Figure 4.

Samples from the Jhumara Formation and Lower and Middle members of the Jhuran Formation exhibit high values of $\varepsilon_{Nd}(t)$, while those from the Upper Member of the Jhuran Formation and the Bhuj Formation demonstrate relatively low $\varepsilon_{Nd}(t)$ values (Fig. 7a). In a cross-plot of $\varepsilon_{Nd}(0)$ versus Th/Sc, samples from Jhumara, Jhuran and Bhuj formation indicate the dominance of felsic components with values similar to those of upper crust (Fig. 8). The fractionation factor $f_{Sm/Nd}$ values vary from −0.37 to −0.49, −0.31 to −0.50 and −0.40 to −0.46 for the Jhumara, Jhuran and Bhuj samples, respectively. Figure 9 shows temporal variations in $\varepsilon_{Nd}(0)$, depleted mantle model age (T_{DM}) and $\varepsilon_{Nd}(t)$ in the succession. The marked decrease of $\varepsilon_{Nd}(0)$ and $\varepsilon_{Nd}(t)$ in samples from the Bhuj Formation is accompanied by an increase in T_{DM}. The T_{DM} age calculated from the measured data range over 1560–2170 Ma, 1430–2220 Ma and 1760–2320 Ma for the Jhumara, Jhuran and Bhuj formations, respectively (Table 6). The average T_{DM} for the analysed samples increases through 1570, 1680 and 1800 Ma from Jhumara through Jhuran and Bhuj formations with T_{DM} mode at 1800 Ma (Fig. 10). In a cross-plot of $f_{Sm/Nd}$ versus $\varepsilon_{Nd}(0)$, Jhumara, Jhuran and Bhuj samples plot within the early Proterozoic upper crustal rocks (> 1.6 Ga) and are in agreement with the values of T_{DM} (Fig. 11).

5. Discussion

Both trace-element analysis and Sr–Nd isotopic composition of sediments in the Mesozoic Kutch Basin point to their derivation primarily from upper continental sources. This is reflected in the enriched LILE and LREE, $(^{87}Sr/^{86}Sr)_t > 0.71$, $\varepsilon_{Nd}(t) < -10$ and negative $f_{Sm/Nd}$ (Condie, 1993). The same is reflected in the T_{DM} distribution of the sediments (Fig. 12). T_{DM} mode at 1800 Ma is related to one of the major crust-forming episodes on the Earth (Condie, 2001; Condie & Aster, 2010). The insignificant change in $\varepsilon_{Nd}(t)$ from the Jhumara Formation to the Middle Member of the Jhuran Formation suggests a negligible shift in sediment sources. The low Th (Fig. 5), lowest $(^{87}Sr/^{86}Sr)_t$ and average T_{DM} age of 1570 Ma indicate sediment inputs from a juvenile mafic source for the oldest Jhumara Formation. The basin possibly received sediments from young orogenic belt(s) during the initial phase. Importantly, the influence of such a sediment source diminishes through time, with felsic (granitic) source progressively dominating from the bottom to the top of the Mesozoic succession. The concentration of trace elements such as Th and Sc, the LREE-enriched chondrite normalized patterns and the negative Eu anomaly suggest the dominance of felsic composition at source for Jhumara, Jhuran and Bhuj formations. The high content of Th (average, 26.4 ppm) and high ΣREE in samples from the Lower Member of the Jhuran Formation are possibly related to the high content of monazite in the samples as reported by Chaudhuri *et al.* (2018) (Table 2). Low Sc/Cr ratios and the cross-plot of La/Th versus Hf indicate a passive-margin setting (Bhatia & Crook, 1986; Floyd & Leveridge, 1987) (Fig. 6).

The depletion of Ba, U, Pb and Sr observed in all the formations (Fig. 2) are possibly linked to the weathering of the source region (cf. Price *et al.* 1991). The magnitude of Sr depletion increases from the bottom to the top of the succession, which could be attributed to higher weathering in the source region as a function of time (i.e. the younger formations received more sediments from highly weathered sources). The highly weathered nature of the source possibly corresponds to the progressive tectonic stability of the basin from syn-rift to post-rift. The two clusters in Nb/Ta versus Zr/Hf cross-plot suggest multiple weathering or depositional histories (Fig. 3). The high Nb/Ta (low Zr/Hf) most likely represents highly recycled sediments, that is, derivation from sedimentary

https://doi.org/10.1017/S0016756820000539 Published online by Cambridge University Press

Table 6. Sm–Nd isotope data for samples from Jhumara, Jhuran and Bhuj formations

Sample	$(^{87}Sr/^{86}Sr)_m$	Rb	Sr	$^{87}Rb/^{86}Sr$	$(^{87}Sr/^{86}Sr)_t$	$(^{143}Nd/^{144}Nd)_m$	$\varepsilon_{Nd}(0)$	Sm	Nd	$^{147}Sm/^{144}Nd$	$f_{Sm/Nd}$	$(^{143}Nd/^{144}Nd)_t$	$\varepsilon_{Nd}(t)$	T_{DM} (Ga)
Bhuj (100 Ma)														
BP-6	0.75989	31.36	32.79	2.77	0.75596	0.51152	−21.8	0.55	2.82	0.1179	−0.40	0.51144	−20.8	2.32
BP-5	0.75716	25.37	25.39	2.89	0.75305	0.51169	−18.5	1.05	5.98	0.1062	−0.46	0.51162	−17.3	1.87
BP-4	0.73392	111.8	84.38	3.83	0.72847	0.51173	−17.7	9.92	56.92	0.1054	−0.46	0.51166	−16.5	1.80
BP-3	0.74542	124.9	60.41	5.98	0.73692	0.51185	−15.4	10.26	54.95	0.1129	−0.43	0.51178	−14.3	1.76
BP-2	0.74698	131.4	59.38	6.40	0.73788	0.51182	−16.0	10.27	55.98	0.1109	−0.44	0.51175	−14.9	1.77
BP-1	0.75807	131.4	45.22	8.41	0.74612	0.51179	−16.5	11.37	62.38	0.1102	−0.44	0.51172	−15.4	1.80
Jhuran (150 Ma)														
NP-18	0.73279	120.1	105.6	3.29	0.72577	0.51187	−15.0	7.04	39.43	0.1079	−0.45	0.51180	−12.6	1.66
NP-17	0.73391	130.7	114.4	3.31	0.72686	0.51187	−15.0	7.00	38.26	0.1106	−0.44	0.51180	−12.6	1.70
NP-16	0.72368	109.6	166.9	1.90	0.71963	0.51186	−15.2	7.64	42.17	0.1095	−0.44	0.51179	−12.8	1.70
NP-15	0.73889	11.28	8.619	3.79	0.73082	0.51185	−15.4	0.66	3.54	0.1127	−0.43	0.51178	−13.1	1.76
NP-14	0.73948	123.4	96.77	3.69	0.73161	0.51184	−15.6	6.29	35.08	0.1084	−0.45	0.51177	−13.2	1.71
NP-13	0.74106	127.7	89.3	4.14	0.73224	0.51187	−15.0	8.95	47.64	0.1136	−0.42	0.51180	−12.7	1.74
NP-12	0.75377	149.8	72.44	5.98	0.74101	0.51179	−16.5	8.64	47.26	0.1105	−0.44	0.51172	−14.2	1.81
NP-11	0.75073	135.6	69.98	5.61	0.73877	0.51173	−17.7	9.21	48.78	0.1142	−0.42	0.51166	−15.4	1.95
NP-10	0.71929	103.3	210.9	1.42	0.71627	0.51196	−13.2	8.55	52.27	0.0989	−0.50	0.51190	−10.7	1.43
NP-9	0.72184	112.4	212.7	1.53	0.71858	0.51188	−14.8	12.31	70.42	0.1057	−0.46	0.51181	−12.4	1.61
NP-8	0.72577	133.6	185.4	2.09	0.72132	0.51190	−14.4	9.52	54.59	0.1054	−0.46	0.51183	−12.0	1.58
NP-7	0.74274	123	81.55	4.36	0.73343	0.51188	−14.8	7.00	39.76	0.1064	−0.46	0.51181	−12.4	1.62
NP-6	0.73694	114.5	87.51	3.79	0.72887	0.51186	−15.2	8.65	48.19	0.1085	−0.45	0.51179	−12.8	1.68
NP-5	0.73776	112.8	86.71	3.76	0.72973	0.51191	−14.2	8.86	48.85	0.1097	−0.44	0.51184	−11.8	1.63
NP-4	0.72949	122.9	144.5	2.46	0.72424	0.51186	−15.2	7.35	40.93	0.1086	−0.45	0.51179	−12.8	1.68
NP-3	0.73493	125	113.9	3.18	0.72816	0.51186	−15.2	9.32	41.38	0.1362	−0.31	0.51177	−13.2	2.22
NP-2	0.72701	148.6	208.6	2.06	0.72261	0.51184	−15.6	10.88	60.80	0.1082	−0.45	0.51177	−13.2	1.70
NP-1	0.72217	110.7	199.7	1.60	0.71875	0.51189	−14.6	8.89	49.64	0.1083	−0.45	0.51182	−12.2	1.64
Jhumara (165 Ma)														
JP-3	0.73402	43.54	97.07	1.30	0.73098	0.51172	−17.9	3.32	16.14	0.1244	−0.37	0.51164	−15.4	2.17
JP-2	0.73174	138.5	85.81	4.67	0.72078	0.51189	−14.6	5.06	29.20	0.1048	−0.47	0.51182	−11.8	1.59
JP-1	0.71899	131.9	204.3	1.87	0.71461	0.51187	−15.0	5.82	34.99	0.1006	−0.49	0.51180	−12.1	1.56

Note: Subscripts m and t indicate the ratios measured and at the time of deposition, respectively. Initial ratios were calculated at the age of deposition, given in brackets. Sm and Nd concentrations were measured by Q-ICP-MS at Physical Research Laboratory, Ahmedabad, India. Depleted mid-ocean-ridge basalt mantle values used for T_{DM} calculations: $^{143}Nd/^{144}Nd = 0.513114$ and $^{147}Sm/^{144}Nd = 0.222$ (Michard *et al.* 1985).

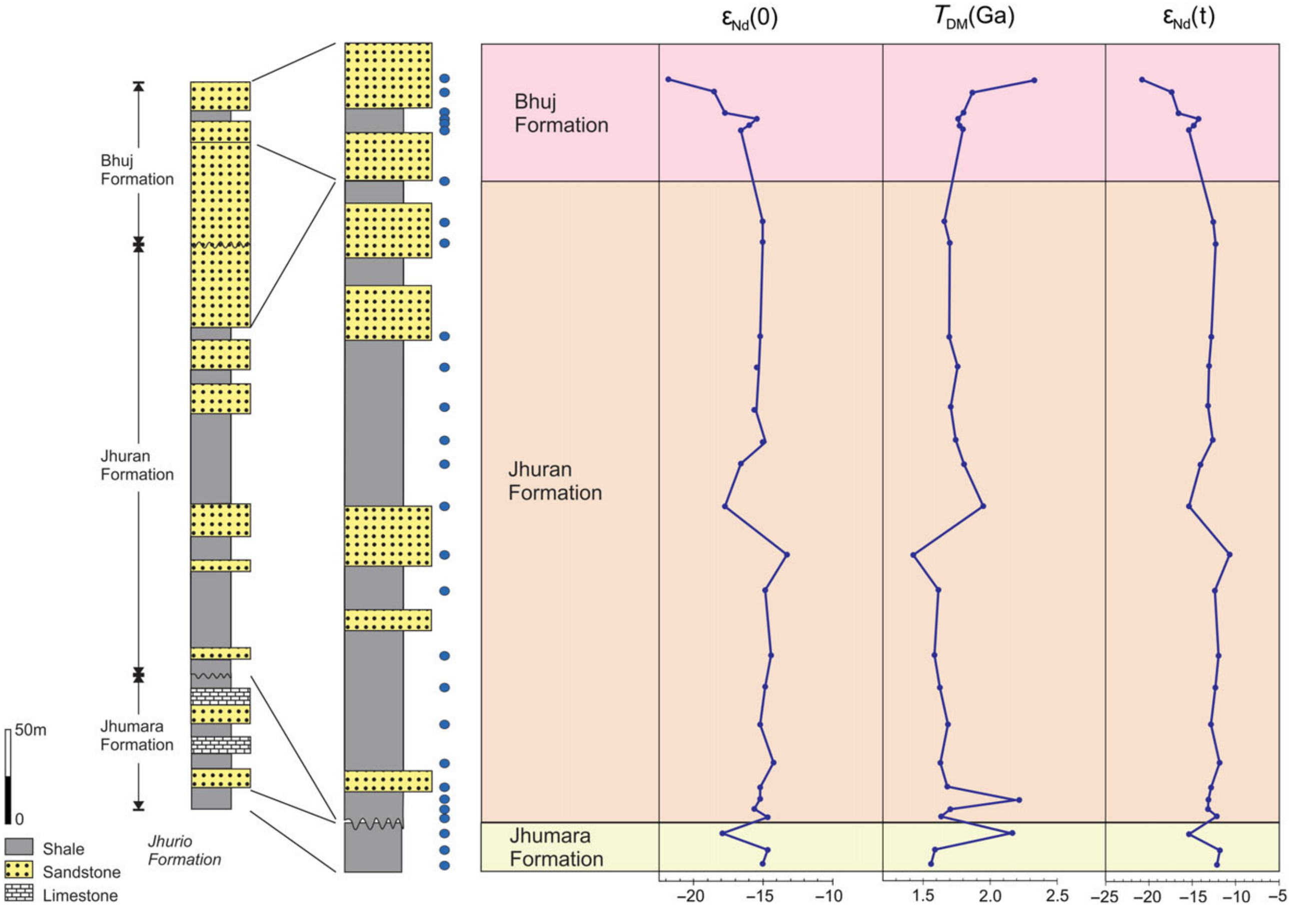

Fig. 9. (Colour online) Variations in $\varepsilon_{Nd}(0)$, T_{DM}(Ga) and $\varepsilon_{Nd}(t)$ across Jhumara, Jhuran and Bhuj formations. Abbreviations as for Figure 4.

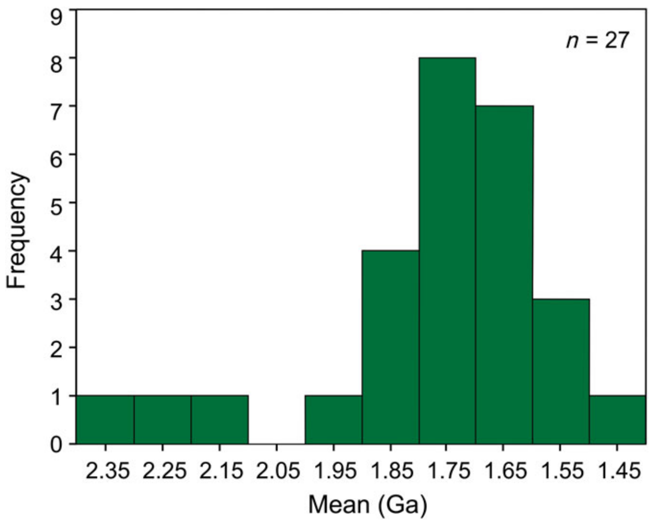

Fig. 10. (Colour online) Histogram of T_{DM} distribution for the sediments in the Mesozoic Kutch Basin.

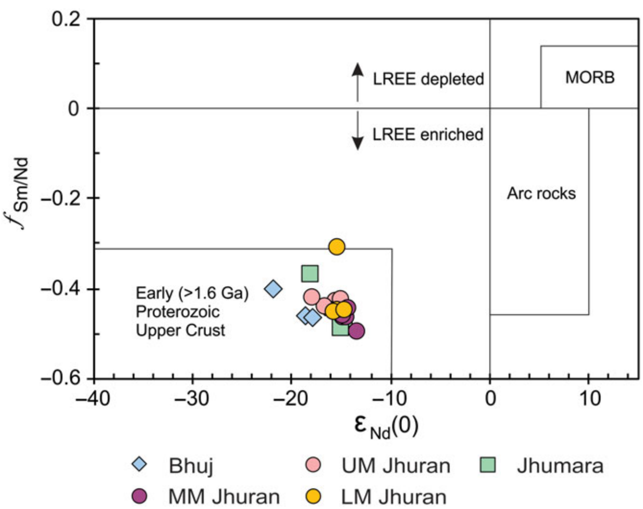

Fig. 11. (Colour online) Plot of $f_{Sm/Nd}$ versus $\varepsilon_{Nd}(0)$ (modified after McLennan *et al.* 1993) for shale samples from Jhumara, Jhuran and Bhuj formations. Abbreviations as for Figure 4.

source rocks; the low Nb/Ta could be attributed to derivation from felsic igneous rocks.

The Nd isotopic composition of the Bhuj Formation indicates predominant sediment derivation from crustal sources of early Proterozoic age (Figs 7, 8, 10–12). T_{DM} ages indicate the dominance of source rocks of late Palaeoproterozoic age (1700–1800 Ma), with subordinate contributions from rocks of early Mesoproterozoic (1400–1600 Ma) and early Palaeoproterozoic (2100–2400 Ma) ages (Fig. 10). The mode of T_{DM} is *c.* 1800 ± 200 Ma.

https://doi.org/10.1017/S0016756820000539 Published online by Cambridge University Press

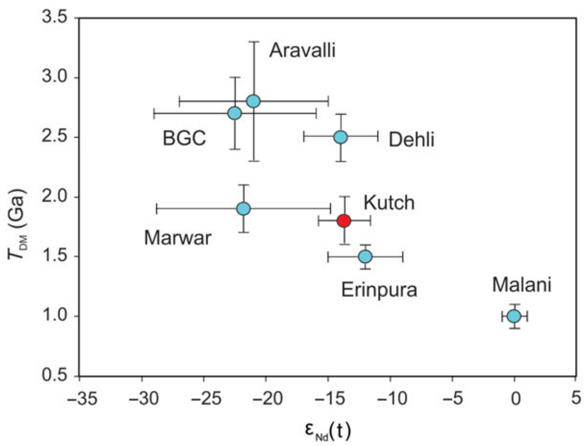

Fig. 12. (Colour online) Average T_{DM} versus average ε_{Nd}(t) plot for Mesozoic sediments in the Kutch Basin compared with those of potential sources in Rajasthan. Error bars for the source points are 3σ. Data sources: George & Ray (2017) and Shukla *et al.* (2019).

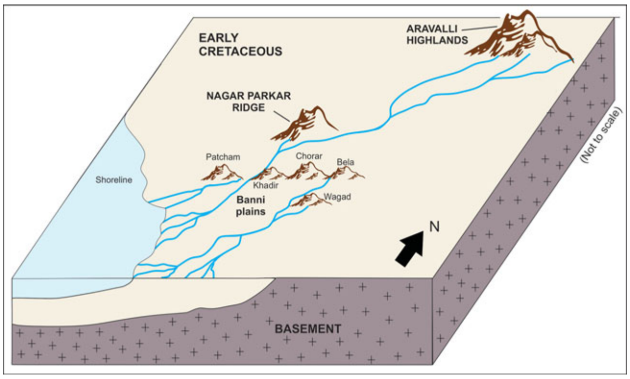

Fig. 13. (Colour online) Schematic diagram of palaeodrainage pattern in the Early Cretaceous Kutch Basin and possible provenance areas.

Considering the overwhelming southwesterly slope of the basin (Biswas, 1991, 2005; Arora *et al.* 2015, 2017; Mandal *et al.* 2016; Desai & Biswas, 2018), the possible rocks which could have sourced these sediments include Nagar Parkar Igneous Suite exposed in the Nagar Parkar Ridge; Banded Gneissic Complex; Aravalli, Bhilwara, Delhi and Marwar supergroups; Erinpura Granite; and Malani volcanic rocks exposed in the Aravalli highlands (Fig. 13). The Nd isotopic composition of Mesozoic sediments in the Kutch Basin and their T_{DM} ages overlap with those of the Proterozoic Marwar Supergroup and the Erinpura Granites (Fig. 12), suggesting these rocks were the major source of sediments to the basin. The mafic juvenile component, especially in the Jhumara Formation, possibly derives from the Nagar Parker Igneous Suite in the north, which contains mafic magmatic rocks within a largely granitic terrain (e.g. Khan *et al.* 2012, 2017; Jan *et al.* 2017; de Wall *et al.* 2018; Rehman *et al.* 2018). This indicates the existence of southerly drainage during the initial phase of the basin. Subsequently, the palaeoslope became southwesterly because of the seawards tilting of the basin. Although there is substantial similarity in the source of the Middle Jurassic syn-rift sediments and the Lower Cretaceous post-rift sediments, trace-element concentrations, their ratios and Nd isotopic compositions reveal subtle variations in source characteristics of younger sediments. The increasing Hf concentration in samples from Jhuran and Bhuj formations exhibiting older sediment components suggest erosional unroofing at the source (Fig. 6). Increasing mean T_{DM} ages exhibited by Jhumara, Jhuran and Bhuj samples further supports this interpretation.

This study indicates the dominance of felsic source rocks for the entire Mesozoic rock record. Integrating results from trace-element and Sr–Nd systematics (low Th, low $(^{87}Sr/^{86}Sr)_t$ and $T_{DM} < 1600$ Ma) highlights additional juvenile mafic source rocks in the Jhumara Formation. The concentration of Hf indicates older source rocks in younger Jhuran and Bhuj formations. Finally, ε_{Nd}(t) and T_{DM} ages, along with the established palaeoslope, provide a more reliable correlation with the existing rocks at source area. This confirms the applicability of trace elements and Nd isotope geochemistry in tracing multiple source rocks.

6. Conclusions

Concentrations of trace elements (Th, Sc) and their ratios (Nb/Ta and Zr/Hf) indicate that multiple sources, including both igneous and sedimentary rocks, contribute sediments to Jhumara, Jhuran and Bhuj formations of the Mesozoic Kutch Basin. High $(^{87}Sr/^{86}Sr)_t$, negative ε_{Nd} and LREE enrichment indicate enriched crustal source of sediments. Although the felsic source rocks dominate, sediments in the Jhumara Formation exhibit inputs from a juvenile mafic source.

T_{DM} ages indicate that rocks of late Palaeoproterozoic age (1700–1800 Ma) are the dominant sediment contributors, as well as those of early Mesoproterozoic (1400–1600 Ma) and early Palaeoproterozoic (2100–2400 Ma) ages.

Concentrations of Hf indicates the dominance of older inputs in younger sediments of Jhuran and Bhuj formations. The increasing mean T_{DM} from bottom to top, namely 1570, 1680 and 1800 Ma for Jhumara, Jhuran and Bhuj formations, respectively, corroborates sediments from older rocks in younger formations, suggesting erosional unroofing of source rocks. Average T_{DM} of 1800 Ma coincides with one of the major crust-forming events.

The increasing $(^{87}Sr/^{86}Sr)_t$ from the bottom to the top of the Mesozoic succession relates to increased weathering of the source rock, possibly linked to the increasing tectonic stability of the basin.

Considering the southwesterly palaeoslope of this basin and the mean T_{DM} ages, rocks of the Marwar Supergroup and Erinpura Granite north and NE of the Kutch Basin constitute the main sediment source. However, minor amount of sediments are derived from the Palaeoproterozoic Banded Gneissic Complex II, Bhilwara Supergroup and Aravalli Supergroup and the Mesoproterozoic Delhi Supergroup. The mafic juvenile component in the sediments of Jhumara Formation is likely to have derived from the Nagar Parkar Igneous Suite to the north.

Acknowledgement. We thank our host institutes for infrastructure support. SB acknowledges the Science and Engineering Research Board, Government of India for financial support through grant no. SR/S4/ES-709/2014 of the Government of India. We also thank Gaurav Chauhan for assistance with sample collection and Emilia Le Pera for constructive suggestions.

References

Ahmad AHM and Bhat GM (2006) Petrofacies, provenance and diagenesis of the Dhosa sandstone member (Chari Formation) at Ler, Kachchh sub-basin, Western India. *Journal of Asian Earth Sciences* **27**, 857–72, https://doi.org/10.1016/j.jseaes.2005.08.005.

Ahmad AHM, Noufal KN, Masroor AM and Khan T (2014) Petrography and geochemistry of Jumara Dome sediments, Kachchh Basin: Implications for provenance, tectonic setting and weathering intensity. *Chinese Journal of Geochemistry* **33**, 9–23, https://doi.org/10.1007/s11631-014-0656-4.

Algeo TJ and Maynard JB (2004) Trace-element behavior and redox facies in core shales of Upper Pennsylvanian Kansas-type cyclothems. *Chemical Geology* **206**, 289–318, https://doi.org/10.1016/j.chemgeo.2003.12.009.

Armstrong-Altrin JS, Botello AV, Villanueva SF and Soto LA (2019) Geochemistry of surface sediments from the northwestern Gulf of Mexico: implications for provenance and heavy metal contamination. *Geological Quarterly* **63**, 522–38.

Armstrong-Altrin JS, Nagarajan R, Madhavaraju J, Rosalez-Hoz L, Lee YI, Balaram V, Cruz-Martínez A and Avila-Ramírez G (2013) Geochemistry of the Jurassic and Upper Cretaceous shales from the Molango Region, Hidalgo, eastern Mexico: Implications for source-area weathering, provenance, and tectonic setting. *Comptes Rendus Geoscience* **345**, 185–202, https://doi.org/10.1016/j.crte.2013.03.004.

Armstrong-Altrin JS, Ramos-Vázquez MA, Zavala-León AC and Montiel-García PC (2018) Provenance discrimination between Atasta and Alvarado beach sands, western Gulf of Mexico, Mexico: Constraints from detrital zircon chemistry and U–Pb geochronology. *Geological Journal* **53**, 2824–48, https://doi.org/10.1002/gj.3122.

Armstrong-Altrin JS and Verma SP (2005) Critical evaluation of six tectonic setting discrimination diagrams using geochemical data of Neogene sediments from known tectonic settings. *Sedimentary Geology* **177**, 115–29, https://doi.org/10.1016/j.sedgeo.2005.02.004.

Arora A, Banerjee S and Dutta S (2015) Black shale in late Jurassic Jhuran Formation of Kutch: Possible indicator of oceanic anoxic event? *Journal of the Geological Society of India* **85**, 265–78, https://doi.org/10.1007/s12594-015-0215-6.

Arora A, Dutta S, Gogoi B and Banerjee S (2017) The effects of igneous dike intrusion on organic geochemistry of black shale and its implications: Late Jurassic Jhuran Formation, India. *International Journal of Coal Geology* **178**, 84–99, doi: 10.1016/j.coal.2017.05.002.

Awasthi N, Ray JS, Laskar AH, Kumar A, Sudhakar M, Bhutani R, Sheth HC and Yadava MG (2010) Major ash eruptions of Barren Island volcano (Andaman Sea) during the past 72 kyr: clues from a sediment core record. *Bulletin of Volcanology* **72**, 1131–36, https://doi.org/10.1007/s00445-010-0408-1.

Awasthi N, Ray JS, Singh AK, Band ST and Rai VK (2014) Provenance of the Late Quaternary sediments in the Andaman Sea: Implications for monsoon variability and ocean circulation. *Geochemistry, Geophysics, Geosystems* **15**, 3890–906, https://doi.org/10.1002/2014GC005462.

Banerjee S, Chattoraj SL, Saraswati PK, Dasgupta S and Sarkar U (2012a) Mineralogy and geochemistry of lagoonal glauconites and their implications on origin and maturation: Oligocene Maniyara Fort Formation, western Kutch, India. *Geological Journal* **47**, 357–71.

Banerjee S, Chattoraj SL, Saraswati PK, Dasgupta S and Sarkar U (2012b) Substrate control on formation and maturation of glauconites in the Middle Eocene Harudi Formation, western Kutch, India. *Marine and Petroleum Geology* **30**, 144–60, https://doi.org/10.1016/j.marpetgeo.2011.10.008.

Bhatia MR and Crook KA (1986) Trace element characteristics of graywackes and tectonic setting discrimination of sedimentary basins. *Contributions to Mineralogy and Petrology* **92**, 181–93.

Biswas SK (1977) Mesozoic rock stratigraphy of Kachchh. *Quarterly Journal of the Geology, Mining and Metallurgy Society of India* **49**, 1–52.

Biswas SK (1980) Mesozoic rock-stratigraphy of Kutch, Gujarat. *Quarterly Journal of Geology, Mining and Metallurgy Society of India* **49**, 1–51.

Biswas SK (1981) Basin framework, palaeo-environment and depositional history of the Mesozoic sediments of Kutch basin, western India. *Quarterly Journal of Geology, Mining and Metallurgy Society of India* **53**, 56–85.

Biswas SK (1982) Rift basins in the western margin of India and their hydrocarbon prospects with special reference to Kutch basin. *AAPG Bulletin* **66**, 1497–513.

Biswas SK (1987) Regional tectonic framework, structure and evolution of the western marginal basins of India. *Tectonophysics* **135**, 307–27.

Biswas SK (1991) Stratigraphy and sedimentary evolution of the Mesozoic basin of Kutch, western India. In *Stratigraphy and Sedimentary Evolution of Western India* (eds SK Tandon, CC Pant, SM Casshyap), pp. 74–103. Nainital: Gyanodaya Prakashan.

Biswas SK (1993) *Geology of Kutch*, Vol. **1**. Dehradun: KDM Institute of Petroleum Exploration, 450 p.

Biswas SK (2005) A review of structure and tectonics of Kutch basin, western India, with special reference to earthquakes. *Current Science* **88**, 1592–600.

Biswas SK and Deshpande (1968) The basement of the Mesozoic sediments of Kutch, Western India. *Bulletin of Geological, Mineral and Metallurgical Society India* **40**, 1–7.

Boynton WV (1984) Cosmochemistry of the rare earth elements: meteorite studies. In *Rare Earth Element Geochemistry* (ed. P Henderson), pp. 63–114. Amsterdam: Elsevier, https://doi.org/10.1016/B978-0-444-42148-7.50008-3.

Chatterjee A and Ray JS (2017) Sources and depositional pathways of mid-Holocene sediments in the Great Rann of Kachchh, India: Implications for fluvial scenario during the Harappan Culture. *Quaternary International* **443**, 177–87, https://doi.org/10.1016/j.quaint.2017.06.008.

Chatterjee A and Ray JS (2018) Geochemistry of Harappan potteries from Kalibangan and sediments in the Ghaggar River: Clues for a dying river. *Geoscience Frontiers* **9**, 1203–11, https://doi.org/10.1016/j.gsf.2017.07.006.

Chaudhuri A, Banerjee S and Chauhan G (2020) Compositional evolution of siliciclastic sediments recording the tectonic stability of a pericratonic rift: Mesozoic Kutch Basin, western India. *Marine and Petroleum Geology* **111**, 476–95, https://doi.org/10.1016/j.marpetgeo.2019.08.026.

Chaudhuri A, Banerjee S and Le Pera E (2018) Petrography of Middle Jurasssic to Early Cretaceous sandstones in the Kutch Basin, western India: Implications on provenance and basin evolution. *Journal of Palaeogeography* **7**, 2–14, https://doi.org/10.1186/s42501-018-0002-6.

Collier JS, Sansom V, Ishizuka O, Taylor RN, Minshull TA and Whitmarsh RB (2008) Age of Seychelles–India break-up. *Earth and Planetary Science Letters* **272**, 264–77, https://doi.org/10.1016/j.epsl.2008.04.045.

Condie KC (1993) Chemical composition and evolution of the upper continental crust: contrasting results from surface samples and shales. *Chemical Geology* **104**, 1–37, https://doi.org/10.1016/0009-2541(93)90140-E.

Condie KC (2001) Continental growth during formation of Rodinia at 1.35-0.9 Ga. *Gondwana Research* **4**, 5–16, https://doi.org/10.1016/S1342-937X(05)70650-X.

Condie KC and Aster RC (2010) Episodic zircon age spectra of orogenic granitoids: the supercontinent connection and continental growth. *Precambrian Research* **180**, 227–36, https://doi.org/10.1016/j.precamres.2010.03.008.

Cullers RL (2002) Implications of elemental concentrations for provenance, redox conditions, and metamorphic studies of shales and limestones near Pueblo, CO, USA. *Chemical Geology* **191**, 305–27, https://doi.org/10.1016/S0009-2541(02)00133-X.

de Wall H, Pandit MK, Donhauser I, Schöbel S, Wang W and Sharma KK (2018) Evolution and tectonic setting of the Malani–Nagarparkar igneous suite: a Neoproterozoic silicic-dominated large igneous province in NW India–SE Pakistan. *Journal of Asian Earth Sciences* **160**, 136–58, https://doi.org/10.1016/j.jseaes.2018.04.016.

Desai BG and Biswas SK (2018) Postrift deltaic sedimentation in western Kachchh Basin: insights from ichnology and sedimentology. *Palaeogeography, Palaeoclimatology, Palaeoecology* **504**, 104–24, https://doi.org/10.1016/j.palaeo.2018.05.013.

Dickin AP (2000) Crustal formation in the Grenville Province: Nd-isotope evidence. *Canadian Journal of Earth Sciences* **37**, 165–81, https://doi.org/10.1139/e99-039.

Dickinson WR (1988) Provenance and sediment dispersal in relation to paleotectonics and paleogeography of sedimentary basins. In *New Perspectives in Basin Analysis* (eds KL Kleinspehn and C Paola), pp. 3–25. New York, NY: Springer, https://doi.org/10.1007/978-1-4612-3788-4_1.

Dickinson WR and Suczek CA (1979) Plate tectonics and sandstone compositions. *AAPG Bulletin* **63**, 2164–82.

Floyd PA and Leveridge BE (1987) Tectonic environment of the Devonian Gramscatho basin, south Cornwall: framework mode and geochemical evidence from turbiditic sandstones. *Journal of the Geological Society* **144**, 531–42, https://doi.org/10.1144/gsjgs.144.4.0531.

Fürsich FT, Singh IB, Joachimski M, Krumm S, Schlirf M and Schlirf S (2005) Palaeoclimate reconstructions of the Middle Jurassic of Kachchh (western India): an integrated approach based on palaeoecological, oxygen isotopic, and clay mineralogical data. *Palaeogeography, Palaeoclimatology, Palaeoecology* **217**, 289–309, doi: 10.1016/j.palaeo.2004.11.026.

George BG and Ray JS (2017) Provenance of sediments in the Marwar Supergroup, Rajasthan, India: Implications for basin evolution and Neoproterozoic global events. *Journal of Asian Earth Sciences* **147**, 254–70, https://doi.org/10.1016/j.jseaes.2017.07.027.

Hofer G, Wagreich M and Neuhuber S (2013) Geochemistry of fine-grained sediments of the upper Cretaceous to Paleogene Gosau Group (Austria, Slovakia): Implications for paleoenvironmental and provenance studies. *Geoscience Frontiers* **4**, 449–68, https://doi.org/10.1016/j.gsf.2012.11.009.

Jan MQ, Agheem MH, Laghari A and Anjum S (2017) Geology and petrography of the Nagar Parkar igneous complex, southeastern Sindh, Pakistan: the Kharsar body. *Journal of the Geological Society of India* **89**, 91–8, https://doi.org/10.1007/s12594-017-0564-4.

Khan T, Murata M, Jan MQ, Rehman HU, Zafar M, Ozawa H, Qadir A and Mehmood S (2017) Felsic dykes in the Neoproterozoic Nagar Parkar Igneous Complex, SE Sindh, Pakistan: geochemistry and tectonic settings. *Arabian Journal of Geosciences* **10**, 308, https://doi.org/10.1007/s12517-017-3077-y.

Khan T, Murata M, Rehman HU, Zafar M and Ozawa H (2012) Nagarparker granites showing Rodinia remnants in the southeastern part of Pakistan. *Journal of Asian Earth Sciences* **59**, 39–51, https://doi.org/10.1016/j.jseaes.2012.05.028.

Mandal A, Koner A, Sarkar S, Tawfik HA, Chakraborty N, Bhakta S and Bose PK (2016) Physico-chemical tuning of palaeogeographic shifts: Bhuj formation, Kutch, India. *Marine and Petroleum Geology* **78**, 474–92, https://doi.org/10.1016/j.marpetgeo.2016.10.003.

McLennan SM, Hemming S, McDaniel DK and Hanson GN (1993) Geochemical approaches to sedimentation, provenance, and tectonics. In *Processes Controlling the Composition of Clastic Sediments* (eds MJ Johnson and A Basu), pp. 21–40. Geological Society of America, Special Paper no. 285.

McLennan SM, Taylor SR and Eriksson KA (1983) Geochemistry of Archean shales from the Pilbara Supergroup, western Australia. *Geochimica et Cosmochimica Acta* **47**, 1211–22, https://doi.org/10.1016/0016-7037(83)90063-7.

Michard A, Gurriet P, Soudant M and Albarede F (1985) Nd isotopes in French Phanerozoic shales: external vs. internal aspects of crustal evolution. *Geochimica et Cosmochimica Acta* **49**, 601–10, doi: 10.1016/0016-7037(85)90051-1.

Nesbitt II W and Young GM (1982) Early Proterozoic climates and plate. *Nature* **299**, 715–17, https://doi.org/10.1038/299715a0.

Price RC, Gray CM, Wilson RE, Frey FA and Taylor SR (1991) The effects of weathering on rare-earth element, Y and Ba abundances in Tertiary basalts from southeastern Australia. *Chemical Geology* **93**, 245–65, https://doi.org/10.1016/0009-2541(91)90117-A.

Ramakrishnan M and Vaidyanadhan R (2008) *Geology of India*, pp. *261–333*. Bangalore: Geological Society of India.

Ramos-Vázquez MA and Armstrong-Altrin JS (2019) Sediment chemistry and detrital zircon record in the Bosque and Paseo del Mar coastal areas from the southwestern Gulf of Mexico. *Marine and Petroleum Geology* **110**, 650–75.

Rehman HU, Khan T, Jan MQ, Lee HY, Chung SL and Murata M (2018) Timing and span of the continental crustal growth in SE Pakistan: evidence from LA-ICP-MS U–Pb zircon ages from granites of the Nagar Parkar Igneous Complex. *Gondwana Research* **61**, 172–86, https://doi.org/10.1016/j.gr.2018.04.018.

Rudnick RL and Gao S (2003) Composition of the continental crust. In *Treatise of Geochemistry* (eds HD Holland and KK Turekian), pp. 1–64. Amsterdam: Elsevier. https://doi.org/10.1016/B0-08-043751-6/03016-4.

Saraswati PK, Khanolkar S and Banerjee S (2018) Paleogene stratigraphy of Kutch, India: an update about progress in foraminiferal biostratigraphy. *Geodinamica Acta* **30**, 100–18, https://doi.org/10.1080/09853111.2017.1408263.

Shukla AD, George BG and Ray JS (2020) Evolution of the Proterozoic Vindhyan Basin, Rajasthan, India: insights from geochemical provenance of siliciclastic sediments. *International Geology Review* 62(2), 153–67, https://doi.org/10.1080/00206814.2019.1594412.

Storey M, Mahoney JJ, Saunders AD, Duncan RA, Kelley SP and Coffin MF (1995) Timing of hot spot-related volcanism and the breakup of Madagascar and India. *Science* **267**, 852–55, https://doi.org/10.1126/science.267.5199.852.

Taylor SR and McLennan SM (1985) *The Continental Crust: Its Composition and Evolution*. Oxford: Blackwell Scientific Publications.

Torsvik TH, Tucker RD, Ashwald LD, Eidea EA, Rakotosolofod NA and De Wite MJ (1998) Late Cretaceous magmatism in Madagascar: palaeomagnetic evidence for a stationary Marion hotspot. *Earth Planetary Science Letters* **164**, 221–32, https://doi.org/10.1016/S0012-821X(98)00206-4.

Tribovillard N, Algeo TJ, Lyons T and Riboulleau A (2006) Trace metals as paleoredox and paleoproductivity proxies: an update. *Chemical Geology* **232**, 12–32, https://doi.org/10.1016/j.chemgeo.2006.02.012.

Valdiya KS (2015) *The Making of India: Geodynamic Evolution*. Heidelberg: Springer.

Verma SP and Armstrong-Altrin JS (2016) Geochemical discrimination of siliciclastic sediments from active and passive margin settings. *Sedimentary Geology* 332, 1–12, https://doi.org/10.1016/j.sedgeo.2015.11.011.

Wedepohl KH (1971) Environmental influences on the chemical composition of shales and clays. *Physics and Chemistry of the Earth* **8**, 305–33, https://doi.org/10.1016/0079-1946(71)90020-6.